

---

# Learning Space Partitions for Path Planning

---

Kevin Yang<sup>1\*</sup> Tianjun Zhang<sup>1\*</sup> Chris Cummins<sup>2</sup> Brandon Cui<sup>2</sup> Benoit Steiner<sup>2</sup>  
Linnan Wang<sup>3</sup> Joseph E. Gonzalez<sup>1</sup> Dan Klein<sup>1</sup> Yuandong Tian<sup>2</sup>  
<sup>1</sup>UC Berkeley <sup>2</sup>Facebook AI Research <sup>3</sup>Brown University  
{yangk,tianjunz,jegonzal,klein}@berkeley.edu  
{cummins,bcui,benoitsteiner,yuandong}@fb.com  
linnan\_wang@brown.edu

## Abstract

Path planning, the problem of efficiently discovering high-reward trajectories, often requires optimizing a high-dimensional and multimodal reward function. Popular approaches like CEM [37] and CMA-ES [16] greedily focus on promising regions of the search space and may get trapped in local maxima. DOO [31] and VOOT [22] balance exploration and exploitation, but use space partitioning strategies independent of the reward function to be optimized. Recently, LaMCTS [45] empirically learns to partition the search space in a reward-sensitive manner for black-box optimization. In this paper, we develop a novel formal regret analysis for when and why such an adaptive region partitioning scheme works. We also propose a new path planning method LaP<sup>3</sup> which improves the function value estimation within each sub-region, and uses a latent representation of the search space. Empirically, LaP<sup>3</sup> outperforms existing path planning methods in 2D navigation tasks, especially in the presence of difficult-to-escape local optima, and shows benefits when plugged into the planning components of model-based RL such as PETS [7]. These gains transfer to highly multimodal real-world tasks, where we outperform strong baselines in compiler phase ordering by up to 39% on average across 9 tasks, and in molecular design by up to 0.4 on properties on a 0-1 scale. Code is available at <https://github.com/yangkevin2/neurips2021-lap3>.

## 1 Introduction

Path planning has been used extensively in many applications, ranging from reinforcement learning [7, 13, 14] and robotics [27, 35, 26] to biology [24], chemistry [40], material design [21], and compiler optimization [42]. The goal is to find the most rewarding trajectory (i.e., state-action sequence)  $\mathbf{x} = (s_0, a_0, s_1, \dots, s_n)$  in the search space  $\Omega$ :  $\mathbf{x}^* = \arg \max_{\mathbf{x} \in \Omega} f(\mathbf{x})$ , where  $f(\mathbf{x})$  is the reward.

In this work, we focus on deterministic path planning problems with long trajectories  $\mathbf{x}$ , and discontinuous and/or multimodal reward functions  $f$ . Such high-dimensional non-convex optimization problems exist in many real domains, both continuous and discrete. While we could always find near-optimal  $\mathbf{x}$  by random sampling given an infinite query budget, in practice we prefer a sample-efficient method that achieves high-reward trajectories with fewer queries of the reward function  $f$ .

While global methods like Bayesian Optimization (BO) [3] may struggle with limited samples and high-dimensional spaces, classic approaches like CEM [37] and CMA-ES [16] learn a local model around promising trajectories. For example, CEM tracks a population of trajectories and repeatedly re-samples its population according to the highest-performing trajectories from the previous generation. On the other hand, such a focus can trap CEM in local optima, as confirmed empirically (Sec. 5).

Other recent approaches, such as VOOT [22] and DOO [31], use a (recursive) region partitioning scheme: they split the search space  $\Omega$  into sub-regions  $\Omega = \Omega_1 \cup \dots \cup \Omega_k$ , then invest more samples into promising sub-regions while continuing to explore other regions via an *upper confidence bound*

(UCB). While such exploration-exploitation procedures adaptively focus on promising sub-regions and lead to sub-linear regret and optimality guarantees, their *region partition* procedure is manually designed by humans and remains non-adaptive. For example, DOO partitions the space with uniform axis-aligned grids and VOOT with Voronoi cells, both independent of the reward  $f$  to be optimized.

Recently, Wang et al. proposed LaNAS [46] and LaMCTS [45], which *adaptively* partition the search regions based on sampled function values, and focus on good regions. They achieve strong empirical performance on Neural Architecture Search (NAS) and black-box optimization, outperforming many existing methods including evolutionary algorithms and BO. Notably, in recent NeurIPS’20 black-box optimization challenges, two teams that use variants of LaMCTS ranked 3rd [38] and 8th [23].

In this paper, we provide a simple theoretical analysis of LaMCTS to reveal the underlying principles of adaptive region partitioning, an analysis missing in the original work. Based on this analysis, we propose **Latent Space Partitions for Path Planning (LaP<sup>3</sup>)**, a novel optimization technique for path-planning. Unlike LaMCTS, LaP<sup>3</sup> uses a latent representation of the search space. Additionally, we use the maximum (instead of the mean) as the node score to improve sample efficiency, verified empirically in Sec. 5.3. Both changes are motivated by our theoretical analysis.

We verify LaP<sup>3</sup> on several challenging path-planning tasks, including 2D navigation environments from past work with difficult-to-escape local optima, and real-world planning problems in compiler optimization and molecular design. In all tasks, LaP<sup>3</sup> demonstrates substantially stronger exploration ability to escape from local optima compared to several baselines including CEM, CMA-ES and VOOT. On compiler phase ordering, we achieve on average 39% and 31% speedup in execution cycles comparing to -O3 optimization and OpenTuner [1], two widely used optimization techniques in compilers. On molecular design, LaP<sup>3</sup> outperforms all of our baselines in generating molecules with high values of desirable properties, beating the best baseline in average property value by up to 0.4 on properties in a [0, 1] range. Additionally, extensive ablation studies show factors that affect the quality of planning and verify the theoretical analysis.

LaP<sup>3</sup> is a general planning technique and can be readily plugged into existing algorithms with path planning components. For example, we apply LaP<sup>3</sup> to PETS [7] in model-based RL and observe substantially improved performance for high-dimensional continuous control and navigation, compared to CEM as used in the original PETS framework.

## 2 Latent Space Monte Carlo Tree Search (LaMCTS)

LaMCTS [45] is recently proposed to solve black-box optimization problems  $\mathbf{x}^* = \arg \max_{\mathbf{x}} f(\mathbf{x})$  via recursively learning  $f$ -dependent region partitions. Fig. 1 and Alg. 1 show the details of LaMCTS as well as our proposed approach LaP<sup>3</sup> (formally introduced in Sec. 4) for comparison.

---

**Algorithm 1** LaP<sup>3</sup> Pseudocode for Path Planning. Improvements over LaMCTS in green.

---

- 1: **Input:** Number of rounds  $T$ , Environment Oracle:  $f(\mathbf{x})$ , **Dataset  $\mathcal{D}$ , Sampling Latent Model  $h(\mathbf{x})$ , Partitioning Latent Model  $s(\mathbf{x})$ .**
  - 2: **Parameters:** Initial #samples  $N_{\text{init}}$ , Re-partitioning interval  $N_{\text{par}}$ , Node partition threshold  $N_{\text{thres}}$ , UCB parameter  $C_p$ .
  - 3: **Pre-train  $h(\cdot)$  on  $\mathcal{D}$  when  $\mathcal{D} \neq \emptyset$ .**
  - 4: Set region partition  $\mathcal{V}_0 = \{\Omega\}$ .
  - 5: Draw  $N_{\text{init}}$  samples uniformly from  $\mathcal{S}_0 = \{(\mathbf{x}_i, f(\mathbf{x}_i))\}_{i=1}^{N_{\text{init}}} \subset \Omega$ .
  - 6: **for**  $t = 0, \dots, T - N_{\text{init}} - 1$  **do**
  - 7:   **if**  $t$  divides  $N_{\text{par}}$  **then**
  - 8:     **Train/fine-tune latent model  $h(\cdot)$  using samples  $\mathcal{S}_t \cup \mathcal{D}$  (Eqn. ??).**
  - 9:     Re-learn region partition  $\mathcal{V}_t \leftarrow \text{Partition}(\Omega, \mathcal{S}_t, N_{\text{thres}}, s(\cdot))$  **in latent space  $\Phi_s$  of  $s(\cdot)$ .**
  - 10:   **end if**
  - 11:   **for**  $k := \text{root}, k \notin \mathcal{V}_{\text{leaf}}$  **do**
  - 12:      $k \leftarrow \arg \max_{\Omega_c \in \text{child}(\Omega_k)} b_c$ , where  $b_c := \left[ \frac{1}{n(\Omega_c)} \sum_{\mathbf{x}_i \in \Omega_c} f(\mathbf{x}_i) \max_{\mathbf{x}_i \in \Omega_c} f(\mathbf{x}_i) + C_p \sqrt{\frac{2 \log n(\Omega_k)}{n(\Omega_c)}} \right]$ .
  - 13:   **end for**
  - 14:   **Initialize CMA-ES using encodings of  $\mathcal{S}_t \cap \Omega_k$  via  $h(\cdot)$ .** Here  $\Omega_k$  is the chosen leaf sub-region.
  - 15:    $\mathcal{S}_t \leftarrow \mathcal{S}_{t-1} \cup \{(\mathbf{x}_t, f(\mathbf{x}_t))\}$ , where  $\mathbf{x}_t$  is **drawn from CMA-ES and decoded via  $h^{-1}(\cdot)$ .**
  - 16: **end for**
-

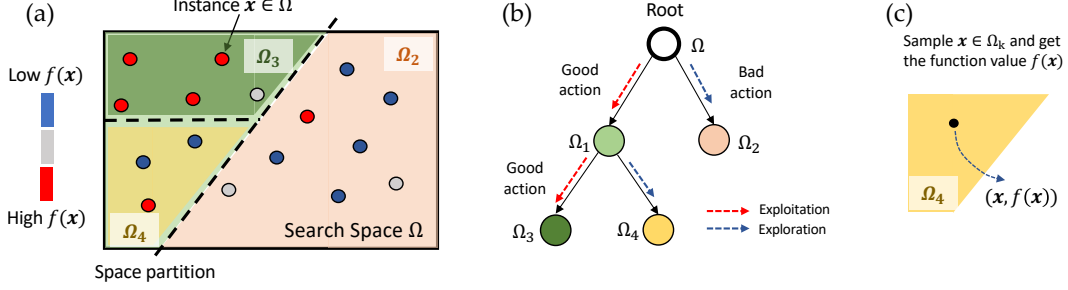


Figure 1: LaP<sup>3</sup> extends LaMCTS [45] to path planning. **(a)** Starting from a search space  $\Omega$ , both LaP<sup>3</sup> and LaMCTS first draw a few samples  $\mathbf{x} \in \Omega$ , then learn to partition  $\Omega$  into a sub-region  $\Omega_1$  with good samples (high  $f(\mathbf{x})$ ) and a sub-region  $\Omega_2$  with bad samples (low  $f(\mathbf{x})$ ). Compared to LaMCTS, LaP<sup>3</sup> uses a *latent space* and reduces the dimensionality of the search space. **(b)** Sampling follows the learned recursive space partition, focusing on good regions while still exploring bad regions using UCB. LaP<sup>3</sup> uses the *maximum* of the sampled value in a region ( $\max_{\mathbf{x}_i \in \Omega} f(\mathbf{x}_i)$ ) as the node value, while LaMCTS uses the mean. **(c)** Upon reaching a leaf, new data points are sampled within the region and the space partition is relearned.

LaMCTS starts with  $N_{\text{init}}$  random samples of the entire search space  $\Omega$  (line 5 in Alg. 1). For a region  $\Omega_k$ , let  $n(\Omega_k)$  be the number of samples within. LaMCTS dictates that, if  $n(\Omega_k) \geq N_{\text{thres}}$ , then  $\Omega_k$  is partitioned into disjoint sub-regions  $\Omega_k = \Omega_{\text{good}} \cup \Omega_{\text{bad}}$  as its *children* (Fig. 1(a)-(b), line 9 in Alg. 1, the function Partition). Intuitively,  $\Omega_{\text{good}}$  contains promising samples with high  $f$ , while  $\Omega_{\text{bad}}$  contains samples with low  $f$ . Unlike DOO and VOOT, such a partition is learned using  $\mathcal{S}_t \cap \Omega_k$ , our samples so far in the region, and is thus dependent on the function  $f$  to be optimized.

Given tree-structured sub-regions, new samples are mostly drawn from promising regions and occasionally from other regions for exploration. This is achieved by Monte Carlo Tree Search (MCTS) [4] (line 11-13): at each tree branching, the UCB score  $b$  is computed to balance exploration and exploitation (line 12). Then the subregion with highest UCB score is selected (e.g., it may have high  $f$  and/or low  $n$ ). This is done recursively until a leaf sub-region  $\Omega'$  is reached. Then a new sample  $\mathbf{x}$  is drawn from  $\Omega'$  (line 15) either uniformly, or from a local model constructed by an existing optimizer (e.g., TuRBO [10], CMA-ES [16]), in which case LaMCTS becomes a meta-algorithm. When more samples are collected, regions are further partitioned and the tree gets deeper.

Finally, the function Partition in Alg. 1 is defined as follows: first a 2-class K-means on  $(\mathbf{x}, f(\mathbf{x}))$  is used to create positive/negative sample groups. Next, a SVM classifier is used to learn the decision boundary (hence the partition), so that samples with high  $f(\mathbf{x})$  fall into  $\Omega_{\text{good}}$ , and samples with low  $f(\mathbf{x})$  fall into  $\Omega_{\text{bad}}$  (Fig. 1(a)). See Appendix A for the pseudo code. The partition boundary can also be re-learned after more samples are collected (line 9).

### 3 A Theoretical Understanding of Space Partitioning

While LaMCTS [45] shows strong empirical performance, it contains several components with no clear theoretical justification. Here we attempt to give a formal regret analysis when sub-regions  $\{\Omega_k\}$  are *fixed* and all at the same tree level, and the function  $f$  is deterministic. We leave further analysis of tree node splitting and evolution of hierarchical structure to future work.

Despite the drastic simplification, our regret bound still shows why an  $f$ -dependent region partition is helpful. By showing that a better regret bound can be achieved by a clever region partition as empirically used in the Partition function in Alg. 1, we justify the design of LaMCTS. Furthermore, our analysis suggests several empirical improvements over LaMCTS and motivates the design of LaP<sup>3</sup>, which outperforms multiple classic approaches on hard path planning problems.

#### 3.1 Regret Analysis with Fixed Sub-Regions

We consider the following setting. Suppose we have  $K$   $d$ -dimensional regions  $\{\Omega_k\}_{k=1}^K$ , and  $n_t(\Omega_k)$  is the visitation count at iteration  $t$ . The global optimum  $\mathbf{x}^*$  resides in some unknown region  $\Omega_{k^*}$ . At each iteration  $t$ , we visit a region  $\Omega_k$ , sample (uniformly or otherwise) a data point  $\mathbf{x}_t \in \Omega_k$ , and retrieve its *deterministic* function value  $f_t = f(\mathbf{x}_t)$ . In each region  $\Omega_k$ , define  $\mathbf{x}_k^* := \arg \max_{\mathbf{x} \in \Omega_k} f(\mathbf{x})$  and the maximal value  $g^*(\Omega_k) = f(\mathbf{x}_k^*)$ . The maximal value *so far* at iteration  $t$  is  $g_t(\Omega_k) = \max_{t' \leq t} f(\mathbf{x}_{t'})$ . It is clear that  $g_t \leq g^*$  and  $g_t \rightarrow g^*$  when  $t \rightarrow +\infty$ .

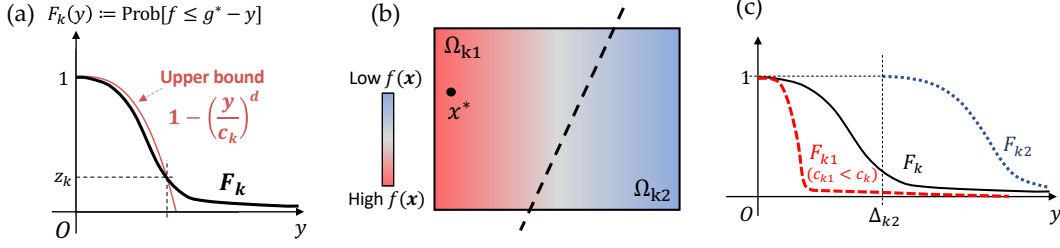


Figure 2: Theoretical understanding of space partitioning. **(a)** Definition of  $(z_k, c_k)$ -diluted region  $\Omega_k$  (Def. 1). **(b)** Partition of region  $\Omega_k$  into good region  $\Omega_{k1}$  and bad region  $\Omega_{k2}$ . Optimal solution  $\mathbf{x}^* \in \Omega_{k1}$ . **(c)** After space partitioning,  $F_k$  is split into  $F_{k1}$  and  $F_{k2}$ . The good region  $F_{k1}$  has much smaller  $c_{k1}$  while the bad region has much larger best-to-optimality gap  $\Delta_{k2}$ . As a result, the expected total regret decreases.

We define the *confidence bound*  $r_t = r_t(\Omega_k)$  so that with high probability, the following holds:

$$g_t(\Omega_k) \geq g^*(\Omega_k) - r_t(\Omega_k) \quad (1)$$

At iteration  $t$ , we pick region  $k_t$  to sample based on the upper confidence bound:  $k_t = \arg \max_k g_t(\Omega_k) + r_t(\Omega_k)$ . Many different confidence bounds can be applied; for convenience in this analysis, we use the “ground truth” bound from the cumulative density function (CDF) of  $f$  within the region  $\Omega_k$  (Please check Appendix B for all proofs):

**Lemma 1.** *Let  $F_k(y) := \mathbb{P}[f(\mathbf{x}) \leq g^*(\Omega_k) - y | \mathbf{x} \in \Omega_k]$  be a strictly decreasing function, and let  $r_{k,t}(\Omega_k) := F_k^{-1}(\delta^{1/n_t(\Omega_k)})$ . Then Eqn. 1 holds with probability  $1 - \delta$ .*

Here  $F_k^{-1}$  is the inverse function of  $F_k$  and randomness arises from sampling within  $\Omega_k$ . Since  $F_k$  is a strictly decreasing function,  $F_k^{-1}$  exists and is also strictly decreasing. By definition,  $F_k \in [0, 1]$ ,  $F_k(0) = 1$  and  $F_k^{-1}(1) = 0$ . We then define the *dilution* of each region as follows:

**Definition 1** ( $(z_k, c_k)$ -dilation). *A region  $\Omega_k$  is  $(z_k, c_k)$ -diluted if there exist  $z_k, c_k$  such that  $F_k(y) \leq 1 - (y/c_k)^d$  for  $y \in [0, c_k(1 - z_k)^{1/d}]$ , where  $z_k$  is the smallest  $F_k(y)$  to make the inequality hold.*

The intuition for dilution for a given region, as depicted in Fig. 2(a), is that all but  $z_k$  fraction of the region has function value close to the maximum, with “close” defined based on  $c_k$  (smaller  $c_k$  implies a stricter definition of “close”). Obviously if  $\Omega_k$  is  $(z_k, c_k)$ -diluted then it is  $(z'_k, c'_k)$ -diluted for any  $c'_k \geq c_k$  and  $z'_k \geq z_k$ . Therefore, we often look for the smallest  $z_k$  and  $c_k$  to satisfy the condition. If a region  $\Omega_k$  has small  $c_k$  and  $z_k$ , we say it is *highly concentrated*. For example, if  $f(\mathbf{x})$  is mostly constant within a region, then  $c_k$  is very small since  $F_k(y)$  drops to 0 very quickly. In such a case, most of the region’s function values are concentrated near the maximum, making it easier to optimize.

While the definition of concentration may be abstract, we show it is implied by Lipschitz continuity:

**Corollary 1.** *If a region  $\Omega_k$  is  $L_k$ -Lipschitz continuous, i.e.,  $|f(\mathbf{x}) - f(\mathbf{x}')| \leq L_k \|\mathbf{x} - \mathbf{x}'\|_2$ , and there exists an  $\epsilon_0$ -ball  $B(\mathbf{x}_k^*, \epsilon_0) \subseteq \Omega_k$ , then with uniform sampling,  $\Omega_k$  is  $(1 - \epsilon_0^d \tilde{V}_k^{-1}, L_k \sqrt[d]{\tilde{V}_k})$ -diluted. Here  $\tilde{V}_k := V_k/V_0$  is the relative volume with respect to the unit sphere volume  $V_0$ .*

Typically, a smoother function (with small  $L_k$ ) and large  $\epsilon_0$  yield a less diluted (and more concentrated) region. However, the concept of dilution (Def. 1) is much broader. For example, if we shuffle function values within  $\Omega_k$ , Lipschitz continuity is likely to break but Def. 1 still holds.

Now we will bound the total regret. Let  $R_t(a_t) := f^* - g_t(\Omega_{a_t}) \geq 0$  be the regret of picking  $\Omega_{a_t}$  and  $R(T) := \sum_{t=1}^T R_t(a_t)$  be the total regret, where  $T$  is the total number of samples (queries to  $f$ ). Define the *gap* of each region  $\Delta_k := f^* - g^*(\Omega_k)$  and split the region indices into  $\mathcal{K}_{\text{good}} := \{k : \Delta_k \leq \Delta_0\}$  and  $\mathcal{K}_{\text{bad}} := \{k : \Delta_k \geq \Delta_0\}$  by a threshold  $\Delta_0$ .

$C_{\text{good}} := \left(\sum_{k \in \mathcal{K}_{\text{good}}} c_k^d\right)^{1/d}$  and  $C_{\text{bad}} := \left(\sum_{k \in \mathcal{K}_{\text{bad}}} c_k^d\right)^{1/d}$  are the  $\ell_d$ -norms of the  $c_k$  in these two sets. Finally,  $M := \sup_{\mathbf{x} \in \Omega} f(\mathbf{x}) - \inf_{\mathbf{x} \in \Omega} f(\mathbf{x})$  is the maximal gap between function values. Treating each region  $\Omega_k$  as an arm and applying a regret analysis similar to multi-arm bandits [41], we obtain the following theorem:

**Theorem 1.** *Suppose all  $\{\Omega_k\}$  are  $(z_k, c_k)$ -diluted with  $z_k \leq \eta/T^3$  for some  $\eta > 0$ . The total expected regret  $\mathbb{E}[R(T)] = \mathcal{O}\left[C_{\text{good}} \sqrt[d]{T^{d-1} \ln T} + M(C_{\text{bad}}/\Delta_0)^d \ln T + KM\eta/T\right]$ .*

### 3.2 Implications of Theorem 1

**The effect of space partitioning.** Reducing  $\{c_k\}$  results in a smaller regret  $R(T)$ . Thus if we can partition  $\Omega_k$  into two sub-regions  $\Omega_{k1}$  and  $\Omega_{k2}$  such that the good partition  $\Omega_{k1}$  has smaller  $c_{k1} < c_k$  and the bad partition  $\Omega_{k2}$  has larger  $\Delta_{k2} > \Delta_0$  and falls into  $\mathcal{K}_{\text{bad}}$ , then we can improve the regret bound (Fig. 2(b)-(c)). This coincides with the Partition function of LaMCTS very well: it samples a few points in  $\Omega_k$ , and trains a classifier to separate high  $f$  from low  $f$ . On the other hand, if we partition a region  $\Omega_k$  randomly, e.g., each  $f(\mathbf{x})$  is assigned to either  $\Omega_{k1}$  or  $\Omega_{k2}$  at random, then statistically  $F_{k1} = F_{k2} = F_k$  and  $c_{k1} = c_{k2} = c_k$ , which *increases* the regret bound. Therefore, the partition needs to be *informed* by data that have already been sampled within the region  $\Omega_k$ .

**Recursive region partitioning.** In Theorem 1, we assume all regions  $\{\Omega_k\}$  have fixed  $c_k$  and  $z_k$ , so the bound breaks for large enough  $T$  (as  $\eta/T^3$  eventually becomes smaller than any fixed  $z_k$ ). However, as LaMCTS conducts further internal partitioning within  $\Omega_k$ , its  $c_k$  and  $z_k$  keep shrinking with more samples  $T$ . If each split leads to slightly fewer bad  $f$  (i.e., lighter “tail”), with the ratio being  $\gamma < 1$ , then by the definition of CDF,  $z_k$  is the probability mass of the tail and thus  $z_k \sim \gamma^{-T/N_{\text{par}}}$ . This would yield  $z_k \leq \eta/T^3$  for all  $T$ , since  $\gamma^{-T}$  decays faster than  $1/T^3$  and Theorem 1 would hold for all  $T$ . See Appendix F.2 for empirical verification of decaying  $z_k$ .

### 3.3 Related Work and Limitations

While related to Lipschitz bandits [28] and coarse-to-fine deterministic function optimization like DOO and SOO [32], our analysis is fundamentally different. We have discussed how  $f$ -dependent region partitioning and a data-driven learning procedure affect the regret bound, which to our knowledge has not been previously addressed. See Appendix B.5 for further remarks on Theorem 1.

There is more work to be done to fully understand how LaMCTS works. In particular, we did not analyze when to split a node (e.g. how many samples we need to collect before making a decision), or the effect of relearning the space partition. We also have not considered stochastic reward functions, where the maximum function value in the sub-region may no longer be the best metric of goodness. We leave these to future work.

## 4 LaP<sup>3</sup> for Path Planning

Based on our analysis, we propose LaP<sup>3</sup>, which extends LaMCTS to path planning, a problem with temporal structure. LaP<sup>3</sup> outperforms baseline path planning approaches in both continuous and discrete path planning problems. Here we represent trajectories as action sequences  $\mathbf{x} = (a_0, a_1, \dots, a_{n-1})$  and treat them as high-dimensional vectors  $\mathbf{x}$  in the trajectory space  $\Omega$ .

Thus, LaP<sup>3</sup> searches over the space  $\Omega$ , recursively partitioning  $\Omega$  into subregions based on trajectory reward, and sampling from subregions using CMA-ES [16] (which is faster than TuRBO [10] used in the original LaMCTS). We emphasize again that LaP<sup>3</sup>’s region partitioning procedure is fully adaptive, in contrast to traditional MCTS approaches such as VOOT, which only partition the trajectory space based on one action at a time.

Additionally, we have made several improvements over the original LaMCTS, as detailed in Algorithm 1. First, we use the maximal value  $\max_{\mathbf{x}_i \in \Omega_k} f(\mathbf{x}_i)$  rather than the mean value  $\frac{1}{n(\Omega_k)} \sum_{\mathbf{x}_i \in \Omega_k} f(\mathbf{x}_i)$  as the metric of goodness for each node  $k$  (and its associated region  $\Omega_k$ ). This is driven by Theorem 1, which gives a regret bound based on maximum values. Intuitively, using the mean value would cause the algorithm to be slow to respond to newly discovered territory: it takes time for the mean metric to boost, and we may miss important leaves. We show the difference empirically in Sec. 5.3.

Second, Theorem 1 suggests that a lower-dimensional (smaller  $d$ ) and smoother (smaller  $c_k$ ) representation leads to lower regret. Therefore, LaP<sup>3</sup> employs a latent space as described below.

### 4.1 Latent Spaces For Partitioning and Sampling

LaP<sup>3</sup> leverages a latent space  $\Phi_s$  for the *partition* space, by passing  $\Omega$  through some encoder  $s$ . That is, we disentangle the *sampling* space  $\Omega$  from which we sample new candidate trajectories, from the *partition* space  $\Phi_s$  on which we construct the search space partition. Critically, we do not need  $s^{-1}$ : we never decode from  $\Phi_s$  back to  $\Omega$ . Thus  $s$  can dramatically reduce the dimension of the partition

space, which may improve regularization due to the small number of samples, without suffering large reconstruction loss.  $s$  will be fixed rather than learned in this case. Once the partition has been constructed on  $\Phi_s$ , and we select a leaf region to propose from, we sample new  $\mathbf{x}$  from  $\Omega$  as before.<sup>1</sup>

In principle, the sampling space can itself be a latent space  $\Phi_h$ , with an encoder  $h$  and decoder  $h^{-1}$ . That is, one runs the inner solver in  $\Phi_h$  to propose samples before decoding back to  $\Omega$ .  $h$  could be a principal component analysis (PCA) [49], a random network encoding [43], or a reversible flow [9], depending on the environment’s particular  $\Omega$  and state/action structure. While some latent representations can be fixed by specifying the inductive bias (e.g., random network encoding), others can be learned from data, optimizing reconstruction loss  $\min_h \mathbb{E}_{\mathbf{x}} [w(\mathbf{x}) \|h^{-1}(h(\mathbf{x})) - \mathbf{x}\|^2]$ , where  $w(\mathbf{x})$  is a weighting function emphasizing trajectories with high cumulative reward  $f(\mathbf{x})$ . In this case,  $h$  and  $h^{-1}$  may be fine-tuned using each new  $(\mathbf{x}, f(\mathbf{x}))$  pair when LaP<sup>3</sup> proposes and queries a new trajectory  $\mathbf{x}$ , or they may be pre-trained using a set of unlabeled  $\mathbf{x}$  with  $w(\mathbf{x}) \equiv 1$ . For consistency in our main experiments, we do not use a latent  $\Phi_h$ , although we observe that using this second latent space can yield a slight performance in some environments (Appendix F.7).

## 5 LaP<sup>3</sup> on Synthetic Environments

We test LaP<sup>3</sup> on a diverse set of environments to evaluate its performance in different settings.

**Baselines.** We compare LaP<sup>3</sup> to several baselines. **LaMCTS** is the original LaMCTS algorithm using CMA-ES as an inner solver, like LaP<sup>3</sup>. **Random Shooting (RS)** [36] samples random trajectories and returns the best one. **Cross-Entropy Methods (CEM)** [2] use the top- $k$  samples to fit a local model to guide future sampling. A related approach, **Covariance matrix adaptation evolution strategy (CMA-ES)** [16], tracks additional variables for improved local model fitting. **Voronoi optimistic optimization applied to trees (VOOT)** [22] is a “traditional” MCTS method for continuous action spaces that builds a tree on actions at each timestep. **iLQR** [26] is a seminal gradient-based local optimization approach used extensively in controls. Finally, **proximal policy optimization (PPO)** [39] is a standard reinforcement learning algorithm.

LaP<sup>3</sup> does not require substantially more tuning effort than CEM or CMA-ES, the best-performing among our baselines experimentally. The only additional hyperparameter tuned in LaP<sup>3</sup> is the  $C_p$  controlling exploration when selecting regions to sample from, which is dependent on the scale of the reward function. However, our  $C_p$  only varies by a factor of up to 10 across our diverse environments, and performance is not overly sensitive to small changes (Appendix F.5).

We use MiniWorld [5] for continuous path planning and MiniGrid [6] for discrete.

### 5.1 MiniWorld

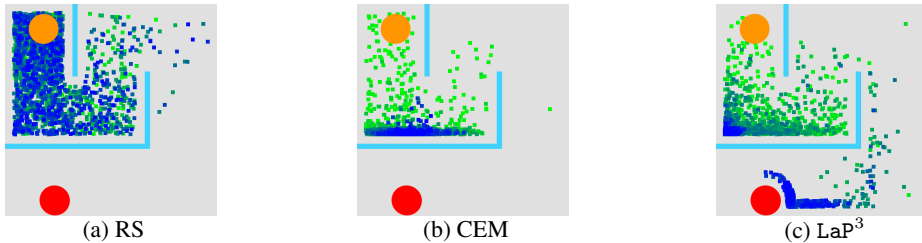


Figure 3: MazeS3 environment. **Start:** Orange circle. **Goal:** Red circle. Dots indicate final agent positions of 2,000 proposed trajectories (green: first iteration, blue: last iteration). CEM gets stuck in a local optimum of reward (shown as concentration of blue dots), while LaP<sup>3</sup> succeeds in reaching the goal.

We consider the following 2D navigation tasks in *MiniWorld*. **MazeS3:** Agent navigates in a 3 by 3 maze to a goal. Greedy path planning gets stuck in local optima (Figure 3). **FourRooms:** Agent navigates from one room in a 2 by 2 configuration to a goal in the diagonally opposite room. Greedy path planning gets stuck in a corner. **SelectObj:** Open space with two goals. Large final reward when

<sup>1</sup>Specifically, we initialize the inner solver (CMA-ES in our experiments) using the pre-existing samples corresponding to the selected leaf region in  $\Phi_s$ , and then propose new samples using that initialization.

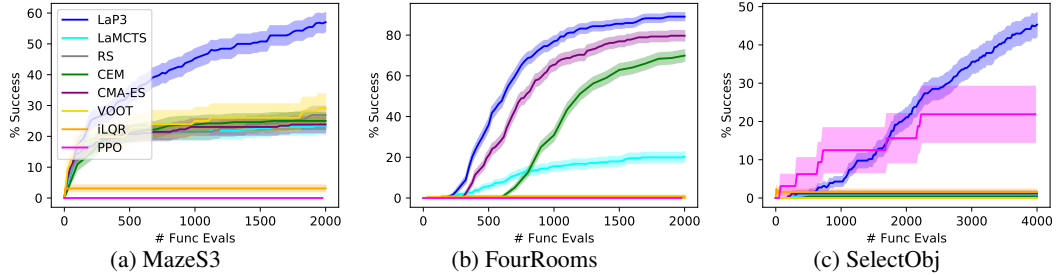


Figure 4: Mean, and standard deviation of mean (256 trials; fewer for VOOT and PPO due to speed), of success rate across MiniWorld tasks. LaP<sup>3</sup> significantly outperforms all baselines on all three tasks.

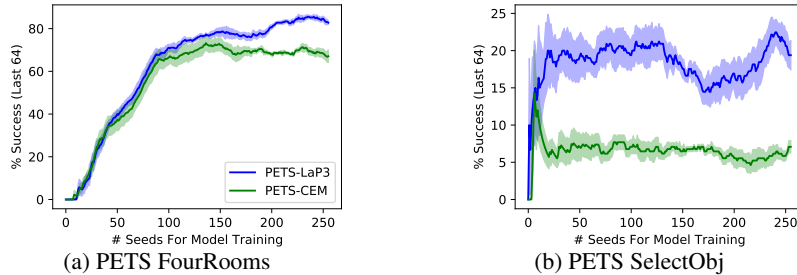


Figure 5: LaP<sup>3</sup> in PETS compared to original PETS planners on MiniWorld environments, using PETS-learned world models. Sliding length-64 window of success percentage against number of training seeds for world model. LaP<sup>3</sup> significantly outperforms all baselines on both tasks.

reaching the farther goal, while a distance-based reward misleadingly points to the closer goal. For full environment specifics, see Appendix H.1.

We modify the original setup to use a continuous action space ( $\Delta x$  and  $\Delta y$ ), and provide a sparse reward (proximity to goal, with an additional bonus for reaching the goal) at end-of-episode. We use a high-dimensional top-down image view as the state. We featurize this image using a randomly initialized convolutional neural network, a reasonable feature extractor as shown in [43]. LaP<sup>3</sup> uses periodic snapshots of the featurized state as the partition space  $\Phi_s$ . That is, we collect all the observed states over the course of the full trajectory, and then form the latent space by concatenating every  $n^{\text{th}}$  state (here  $n = 20$ ), while discarding the rest to reduce overall dimensionality. Success is defined using a binary indicator for reaching the goal (far goal for SelectObj).

**Results.** LaP<sup>3</sup> substantially outperforms all baselines on all three tasks, despite heavily tuning the baselines’ hyperparameters (Appendix G), showing that LaP<sup>3</sup> works for challenging tasks containing suboptimal local maxima. In MazeS3, LaP<sup>3</sup> succeeds but CEM gets stuck (Figure 3). VOOT, which builds an MCTS tree on actions at each timestep, struggles on all environments; LaP<sup>3</sup> can be viewed as an extension of MCTS that performs better on such long-horizon tasks. PPO also performs poorly, perhaps due to the sparse reward given only at the end of an episode, and the relatively small (for RL) number of episodes. In the most difficult SelectObj task, LaP<sup>3</sup> solves nearly half of environment seeds within 4,000 queries of the oracle, whereas most baselines—including the original LaMCTS—quickly reach the near goal but struggle to escape this local optimum.

We also evaluate LaP<sup>3</sup> when combined with a model-based approach, PETS [7], on FourRooms and SelectObj (omitting MazeS3 because the changing maze walls for each seed make it difficult to learn a world model). Following PETS’ setting and due to difficulty in learning image-based world models [12, 14], we use 2D agent position as the state. As shown in Fig. 5, LaP<sup>3</sup> substantially outperforms the authors’ original CEM implementation in the PETS framework, demonstrating that it is not reliant on access to the oracle model but can work with learned models as well.

## 5.2 MiniGrid

*MiniGrid* [6] is a popular sparse-reward symbolic environment for benchmarking RL algorithms. It contains tasks with discrete states and actions such as **DoorKey (DK)**: pick up a key and open

the door connecting two rooms; **MultiRoom (MR)**: traverse several rooms by opening doors; and **KeyCorridor (KC)**, a combination of MR and DK: some doors are locked and require a key. As in MiniWorld, we add proximity to the goal to the final sparse reward.

In discrete action spaces, LaP<sup>3</sup> optimizes the vector of all action probabilities over all timesteps, and takes the highest-probability action at each step. As in MiniWorld, we use periodic state snapshots featurized by a randomly initialized CNN as the partition space  $\Phi_s$ . We compare LaP<sup>3</sup> to the same baselines as in MiniWorld, except VOOT and iLQR which are designed for continuous tasks.

**Results.** LaP<sup>3</sup> is equal to or better than baselines on all six tasks (Table 1). Especially in the hardest tasks with the most rooms (MR-N4S5, MR-N6), LaP<sup>3</sup> improves substantially over baselines.

	DK-6	DK-8	KC-S3R3	KC-S3R4	MR-N4S5	MR-N6
LaMCTS	<b>0.96±0.02</b>	0.09 ± 0.17	-2.63±0.09	-4.43±0.13	-14.71±0.87	-118.70±4.68
RS	<b>0.97±0.01</b>	<b>0.34±0.13</b>	-2.38±0.09	<b>-4.27±0.12</b>	-18.16±0.80	-119.39±4.64
CEM	0.03±0.12	-3.34±0.34	-3.40±0.08	-4.93±0.13	-22.88±1.00	-131.32±5.24
CMA-ES	0.93±0.03	0.23±0.14	-2.46±0.09	-4.44±0.12	-14.31±0.78	<b>-117.50±4.61</b>
LaP <sup>3</sup>	<b>0.95±0.03</b>	<b>0.46±0.13</b>	<b>-2.27±0.09</b>	<b>-4.37±0.13</b>	<b>-11.68±0.75</b>	<b>-113.53±4.49</b>

Table 1: Results for LaP<sup>3</sup> in MiniGrid. LaP<sup>3</sup> is equal or better on all tasks (higher is better).

### 5.3 Analysis

We run several ablations on LaP<sup>3</sup> in MiniWorld to justify our methodological choices. See Appendix F for further analysis on hyperparameter sensitivity, UCB metric, and latent spaces.

**Region Selection in LaP<sup>3</sup>.** We consider four alternative region selection methods. (1) LaP<sup>3</sup>-mean: using mean function value rather than max for UCB, as in LaMCTS [45]; (2) LaP<sup>3</sup>-nolateral: not using a latent space for partitioning; (3) LaP<sup>3</sup>-notree: directly selecting the leaf with the highest UCB score; and (4) LaP<sup>3</sup>-noUCB: only using node value rather than UCB. LaP<sup>3</sup> greatly outperforms all variations in MiniWorld, justifying our design.

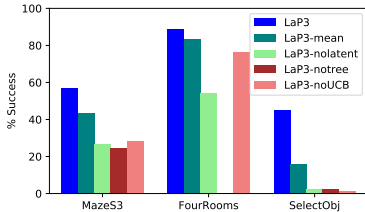


Figure 6: MiniWorld success percentages with different region selection methods.

	MazeS3	FourRooms	SelectObj
$L_k$	87.5	100.0	100.0
$c_k$	81.3	93.8	100.0

Table 2: Percentage out of 32 environment seeds on MiniWorld environments where LaP<sup>3</sup> yields a better estimated Lipschitz and  $c_k$  compared to random partitioning on the same nodes.

**Data-driven space partition in LaP<sup>3</sup> vs. random partitioning.** We examine  $c_k$  in Def. 1 and Lipschitz constant  $L_k$  in Corollary 1 to verify the theory. We conduct a preliminary analysis on LaP<sup>3</sup>'s tree after the full 2,000 queries (4,000 for SelectObj). At each intermediate node, we estimate  $L_k$  and  $c_k$  of its children from the LaP<sup>3</sup> partition, against a random partition that divides the node's samples with the same ratio (see Appendix F.1 for estimation details). We then average the values for both LaP<sup>3</sup> and random partitions over all nodes in the tree. We find that LaP<sup>3</sup> does yield lower average  $L_k$  and  $c_k$  (Table 2), indicating that our data-driven space partition is effective.

## 6 LaP<sup>3</sup> on Real-World Applications

### 6.1 Compiler Phase Ordering

Compiler optimization applies a series of program transformations from a set of predefined optimizations (e.g., *loop invariant code motion*, *function inlining* [30]) to improve code performance. Since these optimizations are not commutative, the order in which they are applied is extremely important. This problem, known as *phase ordering*, is a core challenge in the compiler community. Current



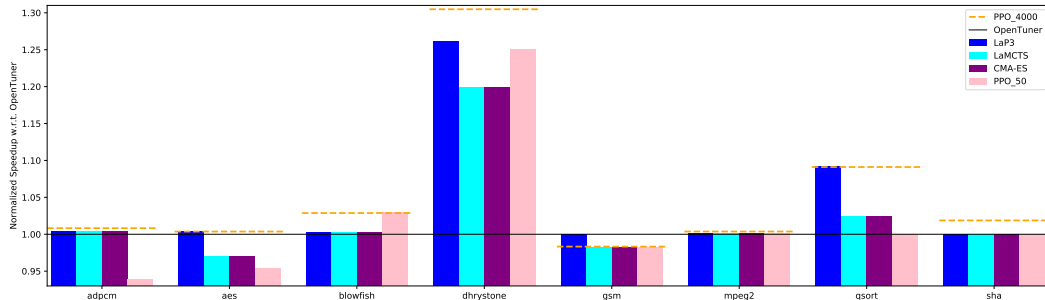


Figure 7: Compiler phase ordering results, in terms of normalized execution cycles with respect to OpenTuner [1], a widely used method for program autotuning. LaP<sup>3</sup> is consistently equal or better compared to baselines. We omitted the matmul task since it doesn’t fit the scale with its 245% speedup over OpenTuner.

solutions to this NP-hard problem rely heavily on heuristics: groups of optimizations are often packed into "optimization levels" (such as -O3 or -O0) hand-picked by developers [34, 42].

We apply LaP<sup>3</sup> to the standard CHStone benchmarks [17], and use periodic snapshots of states as  $\Phi_s$  and the identity as  $\Phi_h$ . See Appendix H.2 for full environment details.

**Results.** LaP<sup>3</sup> is 31% faster on average compared to OpenTuner, and 39% compared to -O3 (not shown in figure). Compared to a stronger PPO baseline using 50 samples (PPO\_50) and to CMA-ES, we achieve up to 10% and 7% speedup respectively. Finally, compared to final PPO results at convergence after 4000 samples (PPO\_4000) as an oracle, LaP<sup>3</sup> does similarly on most tasks, despite being much more sample efficient (only 50 samples). Full results in Appendix E.

## 6.2 Molecular Design

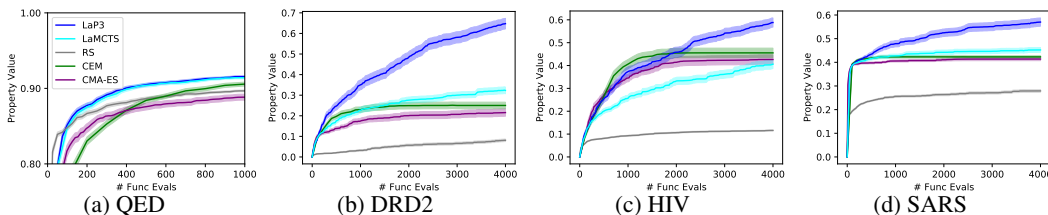


Figure 8: Mean and standard deviation (128 trials), of max property value discovered in molecular design tasks. LaP<sup>3</sup> significantly outperforms all baselines on all properties.

Finally, we evaluate LaP<sup>3</sup> on molecular design. Given an oracle for a desired molecular property, the goal is to generate molecules with high property score after the fewest trials. This is critical to pharmaceutical drug development [44], as property evaluations require expensive wet-lab assays.

Similar to [18], we fix a query budget and optimize several properties: **QED**: a synthetic measure of drug-likeness, relatively simpler to optimize; **DRD2**: a measure of binding affinity to a human dopamine receptor; **HIV**, the probability of inhibition potential for HIV; and **SARS**: the same probability for a variant of the SARS virus, related to the SARS-CoV-2 virus responsible for COVID-19. All four properties have a range of [0, 1]; higher is better. For DRD2, HIV, and SARS, we evaluate using computational predictors from [33] (DRD2) and [51] (HIV, SARS) in lieu of wet-lab assays.

To run LaP<sup>3</sup> on molecular design, we view the molecular string representation (SMILES string [48]) as the action sequence, similar to how many generative models generate molecules autoregressively [11, 25, 8, 50]. Following the state-of-the-art HierG2G model from [19], we learn a latent representation from a subset of ChEMBL [29], a dataset of 1.8 million drug-like molecules, *without* using any of its property labels (e.g., effectiveness in binding to a particular receptor). During this unsupervised training, we only use the 500k molecules with the lowest property scores to ensure a good molecule is discovered by search rather than a simple retrieval from the dataset. Our setting differs from many existing methods for molecular design, which assume a large preexisting set of molecules with the desired property for training the generator [33, 20, 52, 50].

On this task only, the latent space is trained on additional unlabeled data, and is used as both the partition space  $\Phi_s$  and sampling space  $\Phi_h$  for LaP<sup>3</sup>. All baselines operate in the same space for fair comparison. Otherwise, all methods struggle to generate well-formed molecules of reasonable length.

**Results.** Figure 8 shows the highest property score discovered by each method for each property. The absolute difference is small in the relatively simple synthetic QED task. However, LaP<sup>3</sup> outperforms all baselines by a much greater margin—up to 0.4 in DRD2—in the more challenging and realistic DRD2, HIV, and SARS tasks, where CEM and CMA-ES quickly plateau but LaP<sup>3</sup> continues to improve with more function evaluations.

## 7 Conclusion

We propose LaP<sup>3</sup>, a novel meta-algorithm for path planning that learns to partition the search space so that subsequent sampling focuses more on promising regions. We provide a formal regret analysis of region partitioning, motivating improvements that yield large empirical gains. LaP<sup>3</sup> particularly excels in environments with many difficult-to-escape local optima, substantially outperforming strong baselines on 2D navigation tasks as well as real-world compiler optimization and molecular design.

## Acknowledgments and Disclosure of Funding

We thank the members of the Berkeley NLP group as well as our four anonymous reviewers for their helpful feedback. This work was supported by Berkeley AI Research, and the NSF through a fellowship to the first author.

## References

- [1] Jason Ansel, Shoaib Kamil, Kalyan Veeramachaneni, Jonathan Ragan-Kelley, Jeffrey Bosboom, Una-May O’Reilly, and Saman Amarasinghe. Opentuner: An extensible framework for program autotuning. In *Proceedings of the 23rd international conference on Parallel architectures and compilation*, pages 303–316, 2014.
- [2] Zdravko I Botev, Dirk P Kroese, Reuven Y Rubinstein, and Pierre L’Ecuyer. The cross-entropy method for optimization. In *Handbook of statistics*, volume 31, pages 35–59. Elsevier, 2013.
- [3] Eric Brochu, Vlad M Cora, and Nando De Freitas. A tutorial on bayesian optimization of expensive cost functions, with application to active user modeling and hierarchical reinforcement learning. *arXiv preprint arXiv:1012.2599*, 2010.
- [4] Cameron B Browne, Edward Powley, Daniel Whitehouse, Simon M Lucas, Peter I Cowling, Philipp Rohlfshagen, Stephen Tavener, Diego Perez, Spyridon Samothrakis, and Simon Colton. A survey of monte carlo tree search methods. *IEEE Transactions on Computational Intelligence and AI in games*, 4(1):1–43, 2012.
- [5] Maxime Chevalier-Boisvert. gym-miniworld environment for openai gym. <https://github.com/maximecb/gym-miniworld>, 2018.
- [6] Maxime Chevalier-Boisvert and Lucas Willems. Minimalistic gridworld environment for openai gym. <https://github.com/maximecb/gym-minigrid>, 2018.
- [7] Kurtland Chua, Roberto Calandra, Rowan McAllister, and Sergey Levine. Deep reinforcement learning in a handful of trials using probabilistic dynamics models. *NeurIPS*, 2018.
- [8] Hanjun Dai, Yingtao Tian, Bo Dai, Steven Skiena, and Le Song. Syntax-directed variational autoencoder for structured data. *arXiv preprint arXiv:1802.08786*, 2018.
- [9] Laurent Dinh, Jascha Sohl-Dickstein, and Samy Bengio. Density estimation using real nvp. *arXiv preprint arXiv:1605.08803*, 2016.
- [10] David Eriksson, Michael Pearce, Jacob R Gardner, Ryan Turner, and Matthias Poloczek. Scalable global optimization via local bayesian optimization. *arXiv preprint arXiv:1910.01739*, 2019.
- [11] Rafael Gómez-Bombarelli, Jennifer N Wei, David Duvenaud, José Miguel Hernández-Lobato, Benjamín Sánchez-Lengeling, Dennis Sheberla, Jorge Aguilera-Iparraguirre, Timothy D Hirzel,

- Ryan P Adams, and Alán Aspuru-Guzik. Automatic chemical design using a data-driven continuous representation of molecules. *ACS central science*, 4(2):268–276, 2018.
- [12] Danijar Hafner, Timothy Lillicrap, Jimmy Ba, and Mohammad Norouzi. Dream to control: Learning behaviors by latent imagination. *arXiv preprint arXiv:1912.01603*, 2019.
- [13] Danijar Hafner, Timothy Lillicrap, Ian Fischer, Ruben Villegas, David Ha, Honglak Lee, and James Davidson. Learning latent dynamics for planning from pixels. In *International Conference on Machine Learning*, pages 2555–2565. PMLR, 2019.
- [14] Danijar Hafner, Timothy Lillicrap, Mohammad Norouzi, and Jimmy Ba. Mastering atari with discrete world models. *arXiv preprint arXiv:2010.02193*, 2020.
- [15] Ameer Haj-Ali, Qijing Jenny Huang, John Xiang, William Moses, Krste Asanovic, John Wawrzynnek, and Ion Stoica. Autophase: Juggling hls phase orderings in random forests with deep reinforcement learning. *Proceedings of Machine Learning and Systems*, 2:70–81, 2020.
- [16] Nikolaus Hansen. The cma evolution strategy: A tutorial. *arXiv preprint arXiv:1604.00772*, 2016.
- [17] Yuko Hara, Hiroyuki Tomiyama, Shinya Honda, Hiroaki Takada, and Katsuya Ishii. Chstone: A benchmark program suite for practical c-based high-level synthesis. In *2008 IEEE International Symposium on Circuits and Systems*, pages 1192–1195. IEEE, 2008.
- [18] Wengong Jin, Regina Barzilay, and Tommi Jaakkola. Junction tree variational autoencoder for molecular graph generation. In *International Conference on Machine Learning*, pages 2323–2332. PMLR, 2018.
- [19] Wengong Jin, Regina Barzilay, and Tommi Jaakkola. Hierarchical generation of molecular graphs using structural motifs. In *International Conference on Machine Learning*, pages 4839–4848. PMLR, 2020.
- [20] Wengong Jin, Kevin Yang, Regina Barzilay, and Tommi Jaakkola. Learning multimodal graph-to-graph translation for molecular optimization. *arXiv preprint arXiv:1812.01070*, 2018.
- [21] Seiji Kajita, Tomoyuki Kinjo, and Tomoki Nishi. Autonomous molecular design by monte-carlo tree search and rapid evaluations using molecular dynamics simulations. *Communications Physics*, 3(1):1–11, 2020.
- [22] Beomjoon Kim, Kyungjae Lee, Sungbin Lim, Leslie Kaelbling, and Tomas Lozano-Perez. Monte carlo tree search in continuous spaces using voronoi optimistic optimization with regret bounds. *Proceedings of the AAAI Conference on Artificial Intelligence*, 34(06):9916–9924, Apr. 2020.
- [23] Taehyeon Kim, Jaeyeon Ahn, Nakyil Kim, and Seyoung Yun. Adaptive local bayesian optimization over multiple discrete variables. *Workshop at NeurIPS 2020 Competition Track on Black-Box Optimization Challenge*, 2020.
- [24] Christian Kroer and Tuomas Sandholm. Sequential planning for steering immune system adaptation. In *IJCAI*, pages 3177–3184, 2016.
- [25] Matt J Kusner, Brooks Paige, and José Miguel Hernández-Lobato. Grammar variational autoencoder. In *International Conference on Machine Learning*, pages 1945–1954. PMLR, 2017.
- [26] Weiwei Li and Emanuel Todorov. Iterative linear quadratic regulator design for nonlinear biological movement systems. In *ICINCO (1)*, pages 222–229. Citeseer, 2004.
- [27] Thi Thoa Mac, Cosmin Copot, Duc Trung Tran, and Robin De Keyser. Heuristic approaches in robot path planning: A survey. *Robotics and Autonomous Systems*, 86:13–28, 2016.
- [28] Stefan Magureanu, Richard Combes, and Alexandre Proutiere. Lipschitz bandits: Regret lower bound and optimal algorithms. In Maria Florina Balcan, Vitaly Feldman, and Csaba Szepesvári, editors, *Proceedings of The 27th Conference on Learning Theory*, volume 35 of *Proceedings of Machine Learning Research*, pages 975–999, Barcelona, Spain, 13–15 Jun 2014. PMLR.
- [29] David Mendez, Anna Gaulton, A Patrícia Bento, Jon Chambers, Marleen De Veij, Eloy Félix, María Paula Magariños, Juan F Mosquera, Prudence Mutowo, Michał Nowotka, María Gordillo-Marañón, Fiona Hunter, Laura Junco, Grace Mugumbate, Milagros Rodríguez-Lopez, Francis Atkinson, Nicolas Bosc, Chris J Radoux, Aldo Segura-Cabrera, Anne Hersey, and Andrew R Leach. ChEMBL: towards direct deposition of bioassay data. *Nucleic Acids Research*, 47(D1):D930–D940, 11 2018.

- [30] Steven Muchnick et al. *Advanced compiler design implementation*. Morgan kaufmann, 1997.
- [31] Rémi Munos. Optimistic optimization of a deterministic function without the knowledge of its smoothness. In *Proceedings of the 24th International Conference on Neural Information Processing Systems, NIPS'11*, page 783–791, Red Hook, NY, USA, 2011. Curran Associates Inc.
- [32] Rémi Munos. From bandits to monte-carlo tree search: The optimistic principle applied to optimization and planning. 2014.
- [33] Marcus Olivecrona, Thomas Blaschke, Ola Engkvist, and Hongming Chen. Molecular de-novo design through deep reinforcement learning. *Journal of cheminformatics*, 9(1):1–14, 2017.
- [34] Zhelong Pan and Rudolf Eigenmann. Fast and effective orchestration of compiler optimizations for automatic performance tuning. In *International Symposium on Code Generation and Optimization (CGO'06)*, pages 12–pp. IEEE, 2006.
- [35] Nathan Ratliff, Matt Zucker, J Andrew Bagnell, and Siddhartha Srinivasa. Chomp: Gradient optimization techniques for efficient motion planning. In *2009 IEEE International Conference on Robotics and Automation*, pages 489–494. IEEE, 2009.
- [36] Arthur George Richards. *Robust constrained model predictive control*. PhD thesis, Massachusetts Institute of Technology, 2005.
- [37] Reuven Rubinfeld. The cross-entropy method for combinatorial and continuous optimization. pages 127, 190, 1999.
- [38] Mikita Sazanovich, Anastasiya Nikolskaya, Yury Belousov, and Aleksei Shpilman. Solving black-box optimization challenge via learning search space partition for local bayesian optimization. *workshop at NeurIPS 2020 Competition Track on Black-Box Optimization Challenge*, 2020.
- [39] John Schulman, Filip Wolski, Prafulla Dhariwal, Alec Radford, and Oleg Klimov. Proximal policy optimization algorithms. *arXiv preprint arXiv:1707.06347*, 2017.
- [40] Marwin HS Segler, Mike Preuss, and Mark P Waller. Planning chemical syntheses with deep neural networks and symbolic ai. *Nature*, 555(7698):604–610, 2018.
- [41] Aleksandrs Slivkins. Introduction to multi-armed bandits. *arXiv preprint arXiv:1904.07272*, 2019.
- [42] Spyridon Triantafyllis, Manish Vachharajani, Neil Vachharajani, and David I August. Compiler optimization-space exploration. In *International Symposium on Code Generation and Optimization, 2003. CGO 2003.*, pages 204–215. IEEE, 2003.
- [43] Dmitry Ulyanov, Andrea Vedaldi, and Victor Lempitsky. Deep image prior. In *Proceedings of the IEEE conference on computer vision and pattern recognition*, pages 9446–9454, 2018.
- [44] Jessica Vamathevan, Dominic Clark, Paul Czodrowski, Ian Dunham, Edgardo Ferran, George Lee, Bin Li, Anant Madabhushi, Parantu Shah, Michaela Spitzer, et al. Applications of machine learning in drug discovery and development. *Nature Reviews Drug Discovery*, 18(6):463–477, 2019.
- [45] Linnan Wang, Rodrigo Fonseca, and Yuandong Tian. Learning search space partition for black-box optimization using monte carlo tree search. *NeurIPS*, 2020.
- [46] Linnan Wang, Saining Xie, Teng Li, Rodrigo Fonseca, and Yuandong Tian. Sample-efficient neural architecture search by learning actions for monte carlo tree search. *IEEE Transactions on Pattern Analysis and Machine Intelligence*, 2021.
- [47] Tingwu Wang and Jimmy Ba. Exploring model-based planning with policy networks. *arXiv preprint arXiv:1906.08649*, 2019.
- [48] David Weininger. Smiles, a chemical language and information system. 1. introduction to methodology and encoding rules. *Journal of chemical information and computer sciences*, 28(1):31–36, 1988.
- [49] Svante Wold, Kim Esbensen, and Paul Geladi. Principal component analysis. *Chemometrics and intelligent laboratory systems*, 2(1-3):37–52, 1987.
- [50] Kevin Yang, Wengong Jin, Kyle Swanson, Regina Barzilay, and Tommi Jaakkola. Improving molecular design by stochastic iterative target augmentation. In *International Conference on Machine Learning*, pages 10716–10726. PMLR, 2020.

- [51] Kevin Yang, Kyle Swanson, Wengong Jin, Connor Coley, Philipp Eiden, Hua Gao, Angel Guzman-Perez, Timothy Hopper, Brian Kelley, Miriam Mathea, et al. Analyzing learned molecular representations for property prediction. *Journal of chemical information and modeling*, 59(8):3370–3388, 2019.
- [52] Jiaxuan You, Bowen Liu, Rex Ying, Vijay Pande, and Jure Leskovec. Graph convolutional policy network for goal-directed molecular graph generation. *arXiv preprint arXiv:1806.02473*, 2018.

## Checklist

1. For all authors...
  - (a) Do the main claims made in the abstract and introduction accurately reflect the paper’s contributions and scope? **[Yes]** We claim to provide a theoretical explanation of region partitioning and empirical gains over baselines, which are presented in Sec. 3 and Secs. 5,6 respectively.
  - (b) Did you describe the limitations of your work? **[Yes]** We have discussed limitations of our preliminary theory in Sec. 3.2. Our latent spaces also inherently depend on the details of the environments, as described in each individual experiment section. While LaP<sup>3</sup> could be easily modified for black-box optimization in principle, we have made clear that we empirically verify only on path planning.
  - (c) Did you discuss any potential negative societal impacts of your work? **[No]** We do not foresee any obvious negative societal impacts from our work, which contributes a general-purpose path planning algorithm.
  - (d) Have you read the ethics review guidelines and ensured that your paper conforms to them? **[Yes]**
2. If you are including theoretical results...
  - (a) Did you state the full set of assumptions of all theoretical results? **[Yes]** In lemma/theorem statements in Sec. 3.
  - (b) Did you include complete proofs of all theoretical results? **[Yes]** All proofs are in Appendix B.
3. If you ran experiments...
  - (a) Did you include the code, data, and instructions needed to reproduce the main experimental results (either in the supplemental material or as a URL)? **[Yes]** We upload code in the supplementary material.
  - (b) Did you specify all the training details (e.g., data splits, hyperparameters, how they were chosen)? **[Yes]** We discuss all hyperparameter tuning details in Appendix G.
  - (c) Did you report error bars (e.g., with respect to the random seed after running experiments multiple times)? **[Yes]** Included in all experiments in Secs. 5,6.
  - (d) Did you include the total amount of compute and the type of resources used (e.g., type of GPUs, internal cluster, or cloud provider)? **[No]**
4. If you are using existing assets (e.g., code, data, models) or curating/releasing new assets...
  - (a) If your work uses existing assets, did you cite the creators? **[Yes]**
  - (b) Did you mention the license of the assets? **[No]**
  - (c) Did you include any new assets either in the supplemental material or as a URL? **[N/A]** Just code, which is in supplemental material.
  - (d) Did you discuss whether and how consent was obtained from people whose data you’re using/curating? **[No]** We use publicly available datasets/tasks.
  - (e) Did you discuss whether the data you are using/curating contains personally identifiable information or offensive content? **[No]** We don’t use data of this sort.
5. If you used crowdsourcing or conducted research with human subjects...
  - (a) Did you include the full text of instructions given to participants and screenshots, if applicable? **[N/A]**
  - (b) Did you describe any potential participant risks, with links to Institutional Review Board (IRB) approvals, if applicable? **[N/A]**
  - (c) Did you include the estimated hourly wage paid to participants and the total amount spent on participant compensation? **[N/A]**

## A LaMCTS Partition Function

Algorithm 2 details the pseudocode for the partition function used in LaMCTS, which we use in LaP<sup>3</sup> as well.

---

### Algorithm 2 Partition Function

---

```

1: Input: Input Space  $\Omega$ , Samples  $\mathcal{S}_t$ , Node partition threshold  $N_{\text{thres}}$ , Partitioning Latent Model  $s(\mathbf{x})$ 
2: Set  $\mathcal{V}_0 = \{\Omega\}$ 
3: Set  $\mathcal{V}_{\text{queue}} = \{\Omega\}$ 
4: while  $\mathcal{V}_{\text{queue}} \neq \emptyset$  do
5:    $\Omega_p \leftarrow \mathcal{V}_{\text{queue}}.\text{pop}(0)$ 
6:   if  $n(\Omega_p) \geq N_{\text{thres}}$  then
7:      $S_{\text{good}}, S_{\text{bad}} \leftarrow$  samples from  $\mathcal{S}_t$  corresponding to indices of  $k$ -means( $s(\Omega_p \cap \mathcal{S}_t)$ )
8:     Fit SVM on  $S_{\text{good}}, S_{\text{bad}}$ 
9:     Use SVM to split  $\Omega_p$  into  $\Omega_{\text{good}}, \Omega_{\text{bad}}$ 
10:     $\mathcal{V}_0 \leftarrow \mathcal{V}_0 \cup \{\Omega_{\text{good}}, \Omega_{\text{bad}}\}$ 
11:     $\mathcal{V}_{\text{queue}} \leftarrow \mathcal{V}_{\text{queue}} \cup \{\Omega_{\text{good}}, \Omega_{\text{bad}}\}$ 
12:   end if
13: end while
14: return  $\mathcal{V}_0$ 

```

---

## B Proofs

### B.1 Proof of Lemma 1

*Proof.* Let  $\delta < 1$ . Define the following cumulative density function (CDF):

$$F_k(y) := \mathbb{P}[f(\mathbf{x}) \leq g_k^* - y | \mathbf{x} \in \Omega_k] \quad (2)$$

where  $g_k^* := \sup_{\mathbf{x} \in \Omega_k} f(\mathbf{x})$ . It is clear that  $F_k(y)$  is a monotonically decreasing function with  $F_k(0) = 1$  and  $\lim_{y \rightarrow +\infty} F_k(y) = 0$ . Here we assume it is strictly decreasing so that  $F_k(y)$  has a well-defined inverse function  $F_k^{-1}$ .

In the following, we will omit the subscript  $k$  for brevity. Let us bound  $\mathbb{P}[g_t \geq g^* - y]$ :

$$\mathbb{P}[g_t \geq g^* - y] = 1 - \mathbb{P}[g_t \leq g^* - y] \quad (3)$$

$$\stackrel{\textcircled{1}}{=} 1 - \prod_i \mathbb{P}[f(\mathbf{x}_i) \leq g^* - y | \mathbf{x}_i \in \Omega_k] \quad (4)$$

$$= 1 - F_k^{n_t}(y) \quad (5)$$

Note that  $\textcircled{1}$  is due to the fact that all samples  $\mathbf{x}_1, \dots, \mathbf{x}_{n_t}$  are independently drawn within the region  $\Omega_k$ . Given  $\delta$ , let  $r_t := F_k^{-1}(\delta^{1/n_t})$  and we have:

$$\mathbb{P}[g_t \geq g^* - r_t] = 1 - \delta \quad (6)$$

□

### B.2 Proof of Corollary 1

*Proof.* Since  $f$  is  $L_k$ -Lipschitz over region  $\Omega_k$ , we have:

$$|f(\mathbf{x}) - f(\mathbf{x}')| \leq L_k \|\mathbf{x} - \mathbf{x}'\|_2 \quad \forall \mathbf{x}, \mathbf{x}' \in \Omega_k \quad (7)$$

Since the optimal solution  $\mathbf{x}_k^* \in \Omega_k$  is in the interior of  $\Omega_k$ , there exists  $\epsilon_0$  so that  $B(\mathbf{x}_k^*, \epsilon_0) \subseteq \Omega_k$ . From the Lipschitz condition, we know that in the ball  $B(\mathbf{x}_k^*, \epsilon)$  with  $\epsilon \leq \epsilon_0$ , the function values are also quite good:

$$f(\mathbf{x}) \geq f(\mathbf{x}_k^*) - L_k \|\mathbf{x} - \mathbf{x}_k^*\|_2 = g^* - L_k \epsilon, \quad \forall \mathbf{x} \in B(\mathbf{x}_k^*, \epsilon) \quad (8)$$

Therefore, at least in the ball of  $B(\mathbf{x}_k^*, \epsilon)$ , all function values are larger than a threshold  $g^* - L_k \epsilon$ . This means that for  $\epsilon \leq \epsilon_0$ :

$$F_k(L_k \epsilon) = \mathbb{P}[f(\mathbf{x}) \leq g^* - L_k \epsilon | \mathbf{x} \in \Omega_k] \leq 1 - \frac{V_0 \epsilon^d}{V_k} \quad (9)$$

where  $V_0$  is the volume of the unit  $d$ -dimensional sphere. Letting  $\tilde{V}_k := V_k/V_0$  be the relative volume with respect to unit sphere, we have:

$$F_k(y) \leq 1 - \frac{(y/L_k)^d}{\tilde{V}_k} = 1 - \left( \frac{y}{L_k \tilde{V}_k^{1/d}} \right)^d \quad \text{when } y \leq L_k \epsilon_0 \quad (10)$$

Therefore,  $\Omega_k$  is at most  $(1 - \epsilon_0^d \tilde{V}_k^{-1}, L_k \tilde{V}_k^{1/d})$ -diluted with  $z_k = 1 - \epsilon_0^d \tilde{V}_k^{-1}$  and  $c_k = L_k \tilde{V}_k^{1/d}$ .  $\square$

### B.3 New Lemma and Proof

**Lemma 2.** *If  $\Omega_k$  are  $(z_k, c_k)$ -diluted, then for any  $\delta \in [z_k, 1]$  and  $j \geq 1$ , we have:*

$$F_k^{-1}(\delta^{1/j}) \leq c_k \sqrt[d]{\frac{1}{j} \ln \frac{1}{\delta}} \quad (11)$$

*Proof.* Note that the diluted condition  $F_k(y) \leq 1 - \left(\frac{y}{c_k}\right)^d$  for  $y \in [0, c_k \sqrt[d]{1 - z_k}]$  can be also be written as:

$$F_k^{-1}(z) \leq c_k \sqrt[d]{1 - z}, \quad \forall z \in [z_k, 1] \quad (12)$$

Since now we have  $z_k \leq \delta \leq \delta^{1/j} \leq 1$  for any  $j \geq 1$ , following Eqn. 12 we have:

$$F_k^{-1}(\delta^{1/j}) \leq c_k \sqrt[d]{1 - \delta^{1/j}} \quad (13)$$

Due to the inequality that for  $a < 1$  and  $x > 0$ ,  $a^x \geq 1 + x \ln a$  (which can be proven by simply showing the derivative is non-negative), if we take  $a = \delta$  and  $x = 1/j$ , we have:

$$\delta^{1/j} \geq 1 - \frac{1}{j} \ln \frac{1}{\delta} \quad (14)$$

which gives:

$$F_k^{-1}(\delta^{1/j}) \leq c_k \sqrt[d]{j^{-1} \ln 1/\delta} \quad (15)$$

$\square$

### B.4 Proof of Theorem 1

*Proof.* Take  $\delta = \eta/T^3$  so that  $\delta \geq z_k$  for all regions  $\Omega_k$ . Then Eqn. 1 holds for all  $T$  iterations and all  $K$  arms with probability at least  $1 - KT\delta$  by union bound, which we consider a ‘‘good event’’.

For brevity, define  $g_k^* := g(\Omega_k)$  as the optimal function value within the region of  $\Omega_k$  and  $n_{k,t} := n_t(\Omega_k)$  the visitation count of region  $\Omega_k$ . Define  $\Delta_k := f^* - g_k^*$  the minimal regret of each arm and  $r_{k,t} := r_t(\Omega_k)$  the confidence bound. At iteration  $t$ , since we pick  $k = a_t$  as the region to explore, it must be the case that:

$$f^* + r_{k,t} \stackrel{\textcircled{1}}{\geq} g_k^* + r_{k,t} \stackrel{\textcircled{2}}{\geq} g_{k^*,t} + r_{k,t} \stackrel{\textcircled{3}}{\geq} g_{k^*,t} + r_{k^*,t} \stackrel{\textcircled{4}}{\geq} g_{k^*}^* = f^* \quad (16)$$

where  $k^*$  is the index of the optimal region  $\Omega_{k^*}$  where its maximum  $g_{k^*}^*$  is the global optimal value  $f^*$ . Here  $\textcircled{1}$  is due to global optimality of  $f^*$ ,  $\textcircled{2}$  is due to global optimality of  $g_k^*$  within region  $\Omega_k$ :  $g_k^* \geq g_{k,t}$ ,  $\textcircled{3}$  is due to the fact that we pick  $a_t = k$  at iteration  $t$ , and  $\textcircled{4}$  is due to the non-negativity of the confidence bound:  $r_{k^*,t} \geq 0$ . Therefore, since  $g_k^* + r_{k,t} \geq f^*$ , we have:

$$\Delta_k := f^* - g_k^* \leq r_{k,t} \quad (17)$$

Now we bound the total regret.

Note that for  $R_t(a_t) := f^* - g_{a_t,t}$ , we have:

$$R_t(a_t) := f^* - g_{a_t,t} = f^* - g_{a_t}^* + g_{a_t}^* - g_{a_t,t} \leq 2r_{a_t,t} \quad (18)$$



due to the fact that  $\Delta_k = f^* - g_k^* \leq r_{k,t}$  and the property of the confidence bound that  $g_{k,t} \geq g_k^* - r_{k,t}$  with  $k = a_t$ .

One the other hand, using Lemma 2, we also have

$$\Delta_k \leq r_{k,t} = F_k^{-1}(\delta^{1/n_{k,t}}) \leq c_k \sqrt[d]{\frac{1}{n_{k,t}} \ln \frac{1}{\delta}} \quad (19)$$

which means that

$$n_{k,t} \leq \left( \frac{c_k}{\Delta_k} \right)^d \ln \frac{1}{\delta} \quad (20)$$

So if the region  $\Omega_k$  has a large gap  $\Delta_k$ , then  $n_{k,t}$  would have a small upper-bound (and be small). As a result, we would never visit that region after a fixed number of visitations. This also helps bound the regret.

If we sum over  $R_t(a_t)$  over  $t$  iterations, we get  $R(T)$ . We could reorganize them into two kinds of regions, the good regions where  $\mathcal{K}_{\text{good}} := \{k : \Delta_k \leq \Delta_0\}$  and the bad regions where  $\mathcal{K}_{\text{bad}} := \{k : \Delta_k > \Delta_0\}$ :

$$R(T) = \sum_{t=1}^T R_t(a_t) = \underbrace{\sum_{a_t \in \mathcal{K}_{\text{good}}} R_t(a_t)}_{R_{\text{good}}(T)} + \underbrace{\sum_{a_t \in \mathcal{K}_{\text{bad}}} R_t(a_t)}_{R_{\text{bad}}(T)} \quad (21)$$

Let  $M := \sup_{\mathbf{x} \in \Omega} f(\mathbf{x}) - \inf_{\mathbf{x} \in \Omega} f(\mathbf{x})$  be the maximal gap between the highest and lowest function values. Note that  $M$  is also the largest regret for a single move at any iteration. Letting  $C_{\text{bad}} := (\sum_{k \in \mathcal{K}_{\text{bad}}} c_k^d)^{1/d}$  be the  $\ell_d$ -norm of  $c_k$  over bad regions, we then have:

$$R_{\text{bad}}(T) \leq M \left( \frac{C_{\text{bad}}}{\Delta_0} \right)^d \ln \frac{1}{\delta} \quad (22)$$

$$R_{\text{good}}(T) = 2 \sum_{k \in \mathcal{K}_{\text{good}}} \sum_{j=1}^{n_{k,T}} r_{k,t} \Big|_{n_{k,t}=j} = 2 \sum_{k \in \mathcal{K}_{\text{good}}} \sum_{j=1}^{n_{k,T}} F_k^{-1}(\delta^{1/j}) \quad (23)$$

For  $R_{\text{good}}(T)$ , this is because for each region  $k$  we visit it  $n_{k,T}$  times and each time we pay a price that is proportional to  $1/n_{k,t}$  for  $n_{k,t} = 1 \dots n_{k,T}$ .

Using Lemma 2, since all  $\Omega_k$  are  $(z_k, c_k)$ -concentrated and  $z_k \leq \delta$ , this leads to:

$$R_{\text{good}}(T) \leq 2 \sqrt[d]{\ln 1/\delta} \sum_{k \in \mathcal{K}_{\text{good}}} c_k \sum_{j=1}^{n_{k,T}} j^{-1/d} \quad (24)$$

Assuming  $d > 1$  (high-dimensional case), we use the bound

$$\sum_{j=1}^n j^{-1/d} \leq \frac{d}{d-1} n^{1-1/d} \quad (25)$$

and we have:

$$R_{\text{good}}(T) \leq \frac{2d}{d-1} \sqrt[d]{\ln 1/\delta} \sum_{k \in \mathcal{K}_{\text{good}}} c_k n_{k,T}^{\frac{d-1}{d}} \quad (26)$$

Hölder's inequality says if  $1/p + 1/q = 1$ , then  $\sum_k |x_k y_k| \leq (\sum_k |x_k|^p)^{1/p} (\sum_k |y_k|^q)^{1/q}$ . Using it with  $p = d$  and  $q = \frac{d}{d-1}$ , we get

$$R_{\text{good}}(T) \leq \frac{2d}{d-1} \sqrt[d]{\ln \frac{1}{\delta}} \left( \sum_{k \in \mathcal{K}_{\text{good}}} c_k^d \right)^{\frac{1}{d}} \left( \sum_{k \in \mathcal{K}_{\text{good}}} n_{k,T} \right)^{\frac{d-1}{d}} \quad (27)$$

$$\leq \frac{2d}{d-1} \sqrt[d]{\ln \frac{1}{\delta}} C_{\text{good}} T^{\frac{d-1}{d}} \quad (28)$$

where  $C_{\text{good}} := \sum_{k \in \mathcal{K}_{\text{good}}} c_k^d$  is the  $d$ -norm of  $c_k$  over good regions.

Finally, if a good event doesn't happen (with probability  $\frac{1}{T}$ ), we would pay a regret of at most  $MKT^2$  at each iteration, yield a bound of  $MKT^2$  for  $T$  iterations.

Since  $\frac{1}{T} = T^{-3}$  then finally we have

$$E[R(T)] = O\left(C_{\text{good}} \frac{1}{T^{d-1} \ln T} + M \frac{C_{\text{bad}}}{0} \ln T + KM\right) = T \quad (29)$$

□

## B.5 Additional Implications of Theorem 1

Relationship w.r.t sample complexity. Note that one can turn the regret bound  $R(T)$  in Theorem 1 into sample complexity: if there exists  $\mathbf{a}_t$  such that  $E[R(T)] = T$ , then with high probability there exists at least one  $\mathbf{a}_t$  such that  $f(\mathbf{a}_t) = g(\mathbf{a}_t)$ , showing that we already found a good  $\mathbf{a}_t$  with  $f(\mathbf{x}) = g(\mathbf{x})$ . To achieve this, since  $R(T) = T \frac{1}{T^{\frac{d-1}{d}}}$ , we set  $R(T) = T \frac{1}{T^{\frac{d-1}{d}}}$ . Then the sample complexity  $T$  to achieve the global optimum within an  $\epsilon$ -ball is  $\frac{1}{\epsilon^d}$ , which is the best we can achieve without structured information. Previous papers [41] show a slightly worse bound  $O(T^{\frac{d+1}{d+2}})$  since they also consider stochastic functions and discretization error.

Which region to split? Since  $C_{\text{good}} := \sum_{k \in \mathcal{K}_{\text{good}}} c_k^{1-d}$  is an  $d$ -norm, when  $d$  is large (i.e., high-dimensional)  $C_{\text{good}} = \max_{k \in \mathcal{K}_{\text{good}}} c_k$  so ideally we should split the region with the highest  $c_k$  to reduce  $C_{\text{good}}$  the most. Intuitively this means the most diluted / scattered region.

## C Model-Based Reinforcement Learning

LaP<sup>3</sup> can escape local minima and achieve significantly better results in various RL tasks using a simulated environment. In MiniWorld, we showed that we could also plug into the PETS [7] framework, replacing the CEM method that was originally used as a planner (Sec. 5). Here we additionally use Mujoco, a commonly used benchmark, to validate the performance. Note that Mujoco is a very smooth task and doesn't contain many local minima, so traditional methods work reasonably well in this domain. In Tab. 3, we can see that in easier tasks like Reacher and Pusher, LaP<sup>3</sup> is a little worse than CEM. However, in hard tasks like Halfcheetah and Walker, LaP<sup>3</sup> has over 1000 reward gain over baseline methods.

	swimmer	acrobot	hopper	pendulum	halfcheetah
PETS(RS)	12.92 7.92	-41.93 2.17	-1525.39 222.43	130.14 28.39	497.03 121.72
PETS(CEM)	-6.87 1.30	-24.77 7.63	-2102.57 136.35	153.05 12.00	271.01 165.08
LaP <sup>3</sup>	10.82 8.47	6.29 10.29	-1205.01 167.52	153.70 38.02	3942.47 400.01
	reacher	pusher	ant	l-pendulum	walker
PETS(RS)	-1165.59 12.04	-220.58 2.94	1330.81 113.17	-11.87 10.43	-1204.94 344.70
PETS(CEM)	-36.45 2.87	-90.70 7.29	1405.56 46.94	-4.84 5.29	-2036.28 213.41
LaP <sup>3</sup>	-40.31 5.05	-103.42 2.91	1033.46 148.87	-0.30 0.09	-53.25 987.53

Table 3: Results for Mujoco with replanning frequency of 5. We see that LaP<sup>3</sup> performs substantially better than CEM and RS in hard tasks like Halfcheetah and Walker.

## D Evaluation on Synthetic Functions

We additionally evaluate LaP<sup>3</sup> on some synthetic functions (Ackley and Levy functions, both 20-dimensional and 100-dimensional) used in the original LaMCTS paper [45]. For these tasks we compare to just the original LaMCTS method. Both LaP<sup>3</sup> and LaMCTS use the TuRBO inner solver following [45] for the 20-dimensional version of both functions, and the CMA-ES inner solver for

the 100-dimensional version for computational efficiency. LaP<sup>3</sup> performs equal or better on these tasks (Table 4; note lower is better).

	Ackley-20D	Levy-20D	Ackley-100D	Levy-100D
LaMCTS	0.48 ± 0.03	0.51 ± 0.09	0.65 ± 0.25	14.24 ± 4.87
LaP <sup>3</sup>	0.49 ± 0.04	0.34 ± 0.07	0.46 ± 0.15	11.95 ± 3.56

Table 4: LaP<sup>3</sup> vs the original LaMCTS method on some synthetic functions evaluated in the original LaMCTS work. Note *lower* is better. LaP<sup>3</sup> performs equal or better on these tasks.

## E Tables of Numerical Results

We provide in Tables 5 through 9 the numerical final rewards for our tasks, corresponding to the plots in the main text.

	MazeS3	FourRooms	SelectObj
LaMCTS	23.4 ± 2.6	20.3 ± 2.5	0.8 ± 0.6
RS	0.4 ± 0.4	0.0 ± 0.0	3.1 ± 1.1
CMA-ES	23.8 ± 2.7	79.7 ± 2.5	1.2 ± 0.7
CEM	25.0 ± 2.7	69.9 ± 2.9	0.4 ± 0.4
VOOT	26.2 ± 2.7	0.0 ± 0.0	0.0 ± 0.0
RandDOOT	25.0 ± 2.7	0.0 ± 0.0	0.0 ± 0.0
iLQR	3.1 ± 1.1	0.8 ± 0.6	1.6 ± 0.8
PPO	0.0 ± 0.0	0.0 ± 0.0	31.3 ± 8.2
LaP <sup>3</sup>	<b>57.0 ± 3.1</b>	<b>89.1 ± 2.0</b>	<b>45.3 ± 3.1</b>

Table 5: Results (success percentage over 256 trials) for MiniWorld tasks for different methods, querying oracle transition model. LaP<sup>3</sup> substantially outperforms all baselines on all three environments. This table corresponds to Figure 4.

	FourRooms	SelectObj
PETS-RS	0.0 ± 0.0	0.0 ± 0.0
PETS-CEM	66.9 ± 6.3	7.2 ± 1.9
PETS-LaP <sup>3</sup>	<b>83.1 ± 2.3</b>	<b>19.4 ± 1.8</b>

Table 6: Results for MiniWorld tasks for different methods using a learned PETS transition model. The oracle model is only used for final evaluation on each environment seed, and the resulting trajectory becomes future training data to the PETS model. We report the total fraction of environment seeds solved by each method, out of 256 total, averaged across 5 trials. LaP<sup>3</sup> substantially outperforms the original PETS implementation. This table corresponds to Figure 5.

	MazeS3	FourRooms	SelectObj
LaP <sup>3</sup>	<b>57.0 ± 3.1</b>	<b>89.1 ± 2.0</b>	<b>45.3 ± 3.1</b>
LaP <sup>3</sup> -mean	43.4 ± 3.1	83.6 ± 2.3	16.0 ± 2.3
LaP <sup>3</sup> -nolatent	26.6 ± 2.8	54.3 ± 3.1	2.3 ± 0.9
LaP <sup>3</sup> -notree	24.6 ± 2.7	0.0 ± 0.0	2.7 ± 1.0
LaP <sup>3</sup> -noUCB	28.1 ± 2.8	76.6 ± 2.6	1.6 ± 0.8

Table 7: Results for MiniWorld tasks using different region selection methods. 256 trials per method. This corresponds to Figure 6.

	adpcm	aes	blowfish	dhystone	gsm	matmul	mpeg2	qsort	sha
-O0	41260	12633	199345	9258	8130	42085	10489	58400	269653
-O3	16844	9937	188237	5936	7137	33244	8266	52256	226235
PPO_50	11175	10263	<b>175649</b>	5753	6286	<b>9644</b>	8281	52137	209142
OpenTuner	10501	9795	180834	7196	6181	33244	8291	52137	209155
CMA-ES	<b>10451</b>	10093	180198	5996	6294	<b>9644</b>	8280	50869	209142
LaP <sup>3</sup>	<b>10451</b>	<b>9753</b>	180179	5702	<b>6178</b>	<b>9644</b>	8282	<b>47745</b>	209142
PPO_4000	10415	9759	175779	<b>5515</b>	6286	<b>9644</b>	<b>8260</b>	47785	<b>205302</b>

Table 8: Results for compiler phase ordering, in execution cycles for program after a series of transformations, following setup of [15]. 50 oracle accesses per method. This table corresponds to Figure 7.

	QED	DRD2	HIV	SARS
LaMCTS	0.914 ± 0.002	0.323 ± 0.016	0.406 ± 0.019	0.452 ± 0.010
RS	0.897 ± 0.001	0.081 ± 0.006	0.116 ± 0.002	0.279 ± 0.006
CEM	0.906 ± 0.003	0.250 ± 0.016	0.455 ± 0.021	0.423 ± 0.005
CMA-ES	0.888 ± 0.004	0.216 ± 0.018	0.425 ± 0.020	0.414 ± 0.007
LaP <sup>3</sup>	<b>0.916 ± 0.001</b>	<b>0.648 ± 0.026</b>	<b>0.588 ± 0.020</b>	<b>0.570 ± 0.018</b>

Table 9: Mean and standard deviation across 128 random seeds for LaP<sup>3</sup> and baselines on QED, DRD2, SARS, and HIV molecular design tasks; results reported for 1000, 4000, 4000, and 4000 oracle queries respectively. LaP<sup>3</sup> significantly outperforms all three baselines on all four properties. This table corresponds to Figure 8.

## F Detailed Analyses and Ablations

### F.1 $L_k$ and $c_k$ Estimation Details

To loosely approximate the Lipschitz constant in our analysis from Sec. 5.3, we simply check all pairwise Lipschitz constants between existing samples (candidate trajectories) in the tree node (region). Similarly, to loosely approximate  $c_k$ , we take the highest-scoring sample in the region as the “optimum” and estimate  $c_k$  for  $z_k = 0.5$  following our definition using the remaining samples in the region.

### F.2 $z_k$ Estimation

We estimate  $z_k$  over time in our MiniWorld tasks, fixing several different values of  $c_k$  in intervals of 1 reward (Figure 9).  $z_k$  is estimated using 50 samples (in between each dynamic re-partitioning of the space) at each timestep in intervals of 50, with 32 trial runs. In all cases  $z_k$  initially drops very quickly, and then somewhat plateaus after finding the initial local optimum (whether global or not), especially in SelectObj. However, in most cases it still continues to decrease over time.

While this is consistent with our qualitative analysis in Sec. B.5 about how  $z_k$  changes with recursive splitting, in some cases,  $z_k$  seems to stop decreasing over time. Upon inspection, we find that those regions whose  $z_k$  remain high correspond to low-performing regions which do not receive many samples according to UCB exploration. Therefore, such regions won’t improve over time and the  $z_k$  remains high.

### F.3 Latent Space Visualization

We show a t-SNE visualization (Figure 10) of the latent space of trajectories at the end of a sample MazeS3 run of LaP<sup>3</sup>. The first sampled trajectories are colored red, with a gradient toward blue for the later-sampled trajectories. The later trajectories are clearly separated in the latent space.

### F.4 Parameter Space Methods

It is of course possible to optimize the parameters of a policy which outputs an action given the current state, as in the original LaMCTS formulation, or in PPO. Nevertheless, we tune and run a parameter-space version of LaMCTS in the MiniWorld tasks, which is essentially the original

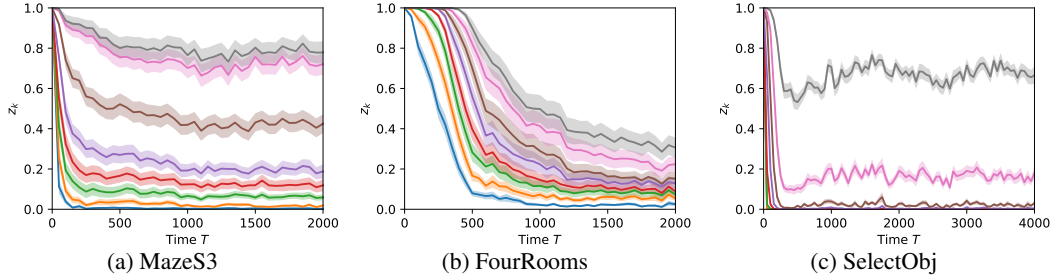


Figure 9: Mean and standard deviation (32 trials), of estimated  $z_k$  for different values of  $c_k$  on MiniWorld tasks.

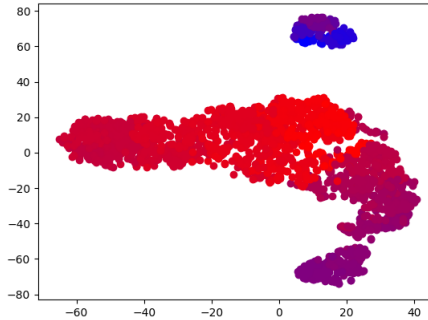


Figure 10: Latent space t-SNE visualization for a sample MazeS3 run of  $\text{LaP}^3$ . Earlier-sampled trajectories (red) are clearly separated from the latest-sampled trajectories (blue).

$\text{LaMCTS}$  adapted to path planning, only with  $\text{TURBO}$  replaced with  $\text{CMA-ES}$  as in  $\text{LaP}^3$  due to speed considerations. Specifically, following  $\text{LaMCTS}$ , we learn the parameters of a linear policy for outputting actions given states.

	<b>MazeS3</b>	<b>FourRooms</b>	<b>SelectObj</b>
$\text{LaMCTS-parameter}$	$10.9 \pm 1.9$	$9.4 \pm 1.8$	$100.0 \pm 0.0$
PPO	$0.0 \pm 0.0$	$0.0 \pm 0.0$	$31.3 \pm 8.2$
$\text{LaP}^3$	$57.0 \pm 3.1$	$89.1 \pm 2.0$	$45.3 \pm 3.1$

Table 10: Comparison of  $\text{LaP}^3$  to an adaptation of the original  $\text{LaMCTS}$ , operating in *parameter* space, on MiniWorld tasks.  $\text{SelectObj}$  is uniquely advantageous to parameter-space methods; for this reason, PPO also performs better than our other baselines (but worse than  $\text{LaP}^3$ ) on that environment only. 256 trials per method.

Working in the parameter space can be clearly advantageous when states are relatively simple and low-dimensional, as in the Mujoco environments evaluated in  $\text{LaMCTS}$  and  $\text{POPLIN}$  [47], or when the policy barely needs to depend on the state at all, as in our  $\text{SelectObj}$  task (Table 10). We designed the  $\text{SelectObj}$  task as a challenge for path planning algorithms operating in the action space, which struggle to escape the local optimum, but in truth this environment can be trivially solved by simply moving in the same correct direction at every step (toward the far goal).

On the other hand, more complex policies may be more challenging to learn when the state representation is higher-dimensional, which may be the case in practical tasks. This is the case in our  $\text{MazeS3}$  and  $\text{FourRooms}$  environments, where the state is represented as a top-down image rather than a vector of position and velocity information. Unlike  $\text{SelectObj}$ , these tasks require navigation around obstacles rather than just moving in a straight line. Despite featurizing with the same randomly initialized CNN as  $\text{LaP}^3$ ,  $\text{LaMCTS-parameter}$  performs very poorly on  $\text{MazeS3}$  and  $\text{FourRooms}$  in comparison. Additionally, methods like  $\text{LaMCTS-parameter}$  which use a parameter space must critically depend on the specific parametric form of the policy to be learned (e.g., whether it is a linear policy, a nonlinear policy parameterized by neural networks, etc); therefore, it is not obvious

how to take advantage of a latent space which encodes a *sequence* of states and/or actions, which is critical in environments such as our molecular design tasks.

### F.5 Hyperparameter Sensitivity Analysis

Since the  $C_p$  parameter is the only additional parameter we tune in LaP<sup>3</sup>, we analyze the sensitivity of LaP<sup>3</sup>'s performance with respect to  $C_p$  on the MiniWorld tasks. Our main results use  $C_p = 2$  except for SelectObj where we used  $C_p = 4$ ; here we run  $C_p = 1, 2, 4$  for all three tasks and show the results in Table 11. LaP<sup>3</sup> even with poorly tuned  $C_p$  values still substantially outperforms CEM on these tasks with difficult-to-escape local optima.

	MazeS3	FourRooms	SelectObj
CEM	25.0 ± 2.7	69.9 ± 2.9	0.4 ± 0.4
LaP <sup>3</sup> - $C_p = 1$	52.7 ± 3.1	89.5 ± 1.9	6.6 ± 1.6
LaP <sup>3</sup> - $C_p = 2$	57.0 ± 3.1	89.1 ± 2.0	23.1 ± 2.6
LaP <sup>3</sup> - $C_p = 4$	53.5 ± 3.1	87.1 ± 2.1	45.3 ± 3.1

Table 11: Results for MiniWorld tasks using different  $C_p$  values for LaP<sup>3</sup>.  $C_p = 2$  corresponds to our main paper results, except for SelectObj where we used  $C_p = 4$ . LaP<sup>3</sup> is relatively insensitive to changes in  $C_p$  on MazeS3 and FourRooms and only more sensitive on the more difficult SelectObj task. However, even poorly tuned versions of LaP<sup>3</sup> outperform CEM, reproduced for baseline comparison. 256 trials per method.

### F.6 Max vs. Mean UCB Metric For MCTS

Our theory suggests that the UCB metric for MCTS should be based on the max function value rather than the mean for the deterministic functions that we consider in this work. Figure 6 already shows this for MiniWorld; here we show the max vs. mean analysis for all tasks in Tables 12, 13, 14, and 15.

	MazeS3	FourRooms	SelectObj
LaP <sup>3</sup> -mean	43.4 ± 3.1	83.6 ± 2.3	16.0 ± 2.3
LaP <sup>3</sup>	57.0 ± 3.1	89.1 ± 2.0	45.3 ± 3.1

Table 12: Results for LaP<sup>3</sup> (using max function value for UCB) in MiniWorld compared to LaP<sup>3</sup> using the mean function value metric for UCB. LaP<sup>3</sup> is substantially better. 256 trials per method.

	DK-6	DK-8	KC-S3R3	KC-S3R4	MR-N4S5	MR-N6
LaP <sup>3</sup> -mean	0.98 ± 0.02	0.25 ± 0.13	-2.36±0.09	-4.36±0.12	-11.78 ± 0.77	-114.63 ± 4.53
LaP <sup>3</sup>	0.95±0.03	0.46±0.13	-2.27±0.09	-4.37±0.13	-11.68±0.75	-113.53±4.49

Table 13: Results for LaP<sup>3</sup> (using max function value for UCB) in MiniGrid compared to LaP<sup>3</sup> using the mean function value metric for UCB. LaP<sup>3</sup> performs similarly or better. 256 trials per method.

	adpcm	aes	blowfish	dhystone	gsm	matmul	mpeg2	qsort	sha
LaP <sup>3</sup> -mean	10501	10407	176429	5740	6305	8841	8281	47745	209142
LaP <sup>3</sup>	10451	9753	180179	5702	6178	9644	8282	47745	209142

Table 14: Results for LaP<sup>3</sup> (using max function value for UCB) in compiler phase ordering compared to LaP<sup>3</sup> using the mean function value metric for UCB. The two versions perform similarly. 256 trials per method.

### F.7 Latent Space Ablations

We conduct additional analysis on the use of a latent partition space  $\Phi_s$  in the MiniWorld, MiniGrid, and compiler phase ordering tasks in Tables 16 (reproduced from Table 7), 17, and 18 respectively.

	<b>QED</b>	<b>DRD2</b>	<b>HIV</b>	<b>SARS</b>
LaP <sup>3</sup> -mean	0.914 ± 0.002	0.323 ± 0.016	0.406 ± 0.019	0.452 ± 0.010
LaP <sup>3</sup>	0.916 ± 0.001	0.648 ± 0.026	0.588 ± 0.020	0.570 ± 0.018

Table 15: Results for LaP<sup>3</sup> (using max function value for UCB) in molecular design tasks compared to LaP<sup>3</sup> using the mean function value metric for UCB. LaP<sup>3</sup> performs similarly on the easiest QED task and substantially better on the others. 256 trials per method.

	<b>MazeS3</b>	<b>FourRooms</b>	<b>SelectObj</b>
LaP <sup>3</sup> -nolotent	26.6 ± 2.8	54.3 ± 3.1	2.3 ± 0.9
LaP <sup>3</sup>	57.0 ± 3.1	89.1 ± 2.0	45.3 ± 3.1

Table 16: Results for LaP<sup>3</sup> in MiniWorld compared to LaP<sup>3</sup> without the use of a partition latent space  $\Phi_s$ . LaP<sup>3</sup> is substantially better. 256 trials per method.

	<b>DK-6</b>	<b>DK-8</b>	<b>KC-S3R3</b>	<b>KC-S3R4</b>	<b>MR-N4S5</b>	<b>MR-N6</b>
LaP <sup>3</sup> -nolotent	0.98±0.02	0.25±0.13	-2.36±0.09	-4.36±0.12	-11.78±0.77	-114.63±4.53
LaP <sup>3</sup>	0.95±0.03	0.46±0.13	-2.27±0.09	-4.37±0.13	-11.68±0.75	-113.53±4.49

Table 17: Results for LaP<sup>3</sup> in MiniGrid compared to LaP<sup>3</sup> without the use of a partition latent space  $\Phi_s$ . LaP<sup>3</sup> is better in most cases. 256 trials per method.

	<b>adpcm</b>	<b>aes</b>	<b>blowfish</b>	<b>dhystone</b>	<b>gsm</b>	<b>matmul</b>	<b>mpeg2</b>	<b>qsort</b>	<b>sha</b>
LaP <sup>3</sup> -nolotent	10451	10263	176429	6617	6169	8841	8280	52137	476269
LaP <sup>3</sup>	10451	9753	180179	5702	6178	9644	8282	47745	209142

Table 18: Results for LaP<sup>3</sup> in compiler phase ordering compared to LaP<sup>3</sup> without the use of a partition latent space  $\Phi_s$ . The two versions are comparable in most cases.

LaP<sup>3</sup> performs similarly or better compared to the version without a latent space; the difference is especially large in MiniWorld.

Additionally, it is possible to use a separate sampling latent space  $\Phi_h$ , as illustrated here in MiniGrid (Table 19), although we do not do so in our main results to keep consistency between latent spaces across tasks. The version with a latent space (a reversible flow model here) performs slightly better.

	<b>DK-6</b>	<b>DK-8</b>	<b>KC-S3R3</b>	<b>KC-S3R4</b>	<b>MR-N4S5</b>	<b>MR-N6</b>
LaP <sup>3</sup> -latent $\Phi_h$	0.97±0.02	0.48±0.11	-2.19±0.15	-4.22±0.13	-10.68±0.68	-112.72±4.46
LaP <sup>3</sup>	0.95±0.03	0.46±0.13	-2.27±0.09	-4.37±0.13	-11.68±0.75	-113.53±4.49

Table 19: Results for LaP<sup>3</sup> in MiniGrid compared to LaP<sup>3</sup> with the use of a sampling latent space. While the differences are small on most cases, LaP<sup>3</sup> with a latent  $\Phi_h$  is better on all tasks. 256 trials per method.

We additionally ablate on the latent space (used for both partitioning and sampling) in the easiest of our molecular design tasks, the QED property. Specifically, we build the molecular SMILES string autoregressively, using a discrete action space with 10 choices: the 9 most common characters in molecular SMILES strings, in addition to an end token. (We limit the space of possible characters in order to increase the chances of generating well-formed SMILES strings.) We optimize in a continuous space of action probabilities as in MiniGrid, and allow a maximum length of 50 characters.

The poor results demonstrate the absolute *necessity* of a latent space in the molecular design task (Table 20). While typical molecular SMILES strings for this task are 30 to 50 characters long, both LaP<sup>3</sup> and baselines struggle to generate well-formed strings even of length 3 to 5 without the pre-trained latent space. Accordingly, the performance is drastically lower for all methods.

QED	
RS-no $\Phi$	0.417 $\pm$ 0.002
CEM-no $\Phi$	0.411 $\pm$ 0.002
CMA-ES-no $\Phi$	0.403 $\pm$ 0.003
LaP <sup>3</sup> -no $\Phi$	0.416 $\pm$ 0.003
RS	0.897 $\pm$ 0.001
CEM	0.906 $\pm$ 0.003
CMA-ES	0.888 $\pm$ 0.004
LaP <sup>3</sup>	0.916 $\pm$ 0.001

Table 20: Mean and standard deviation across 128 random seeds for LaP<sup>3</sup> and baselines on QED, with and without the pre-trained latent space.

## F.8 Other Inner Solvers

In this work we have used CMA-ES as the inner solver due to its speed and acceptable performance. The original LaMCTS work used the TuRBO solver [10], which is prohibitively slow for many of our experiments. Nevertheless, we have run experiments on the MiniWorld tasks using a smaller number of trials to check performance using an alternate inner solver, both on LaP<sup>3</sup> and also on the LaMCTS baseline (Table 21). In most cases TuRBO performs equal or worse; we hypothesize this is because our tasks use a smaller query budget per trial compared to the original LaMCTS work, causing TuRBO to use too large a fraction of its total budget in each inner loop.

	MazeS3	FourRooms	SelectObj
LaMCTS-TuRBO	21.9 $\pm$ 7.3	0.0 $\pm$ 0.0	0.0 $\pm$ 0.0
LaMCTS	23.4 $\pm$ 2.6	20.3 $\pm$ 2.5	0.8 $\pm$ 0.6
LaP <sup>3</sup> -TuRBO	52.2 $\pm$ 10.4	63.6 $\pm$ 14.5	47.1 $\pm$ 12.1
LaP <sup>3</sup>	57.0 $\pm$ 3.1	89.1 $\pm$ 2.0	45.3 $\pm$ 3.1

Table 21: Results for LaP<sup>3</sup> and LaMCTS with CMA-ES and TuRBO inner solvers in MiniWorld, with fewer trials for TuRBO due to computational expense. TuRBO generally performs equal or worse on this task.

## G Baseline Details and Hyperparameter Tuning

**LaP<sup>3</sup>.** For our method, we try  $C_p$  in  $\{0.5, 1, 2, 4\}$ . If the search space is not explicitly bounded, we sample the first  $N_{init}$  points used to initialize the partition tree using the same  $\sigma$  as CEM. Note  $N_{init}$  is not tuned; we use 5 for compiler phase optimization where our query budget is only 50, and 50 elsewhere. No other hyperparameters are tuned.

**LaMCTS.** Detailed in Algorithm 1, where we summarize the changes made in LaP<sup>3</sup> compared to LaMCTS. It is tuned similarly to our own method LaP<sup>3</sup>.

**RS.** The simplest baseline, in which one simply samples random trajectories and in the end returns the best-performing among them. We do not tune this baseline.

**CEM.** An evolutionary method which tracks a population of  $N$  samples. At each step, it selects the best  $N_e$  samples from its population to initialize the mean  $\mu$  for the next generation of  $N$  samples, drawn from a Gaussian distribution with standard deviation  $\sigma$ . However, while too-small  $\sigma$  may prevent CEM from escaping local optima, too-large  $\sigma$  may yield results little better than random shooting. We find that the choice of  $\sigma$  is critical to CEM’s performance in our test environments. Therefore, we systematically tune  $\sigma$  when running CEM in all environments (checking  $\{1, 2, 4, 8\}$ ). While other parameters such as  $N$  and  $N_e$  are also tunable, we find that these make a smaller difference, so we did not tune them extensively.

**CMA-ES.** A more complex evolutionary method which can be viewed as a variant of CEM. After providing an initial  $\mu$  and  $\sigma$  for the first generation, CMA-ES determines its own  $\sigma$  automatically afterward, while also fitting additional parameters. Even so, we find that its performance is highly sensitive to the initial  $\sigma$ , and we tune this parameter in the same way that we do for CEM.



**VOOT.** An MCTS method which builds a tree on actions. We tune the exploration parameter in the VOO submodule, trying values in  $\{0.1, 0.3, 0.5\}$ .

**RandDOOT.** An MCTS method which builds a tree on actions similar to VOOT, but which splits using axis-aligned boundaries rather than splitting into Voronoi regions; used as a baseline in their original paper [22]. We did not tune hyperparameters.

**iLQR.** A gradient-based optimization method for continuously optimizing the planned trajectory, which we run to convergence. It cannot easily escape local optima. As the performance was relatively insensitive to hyperparameters, we did not systematically tune.

**PPO.** A standard reinforcement learning algorithm which operates in the parameter space, unlike our other baselines. Since PPO is relatively robust to hyperparameters [39], we didn't systematically tune.

## H Additional Environment Details

### H.1 MiniWorld

We modified the original MiniWorld environments to have continuous action spaces and to have more consistent difficulty across random seeds, as follows.

**MazeS3.** A 3x3 maze of rooms which are each 3 units by 3 units, with walls between rooms being 0.25 units wide. The maze is constructed by recursive backtracking from the top left room. The agent begins in the top left room and the goal is placed in the last room generated in the maze construction. The step size is 0.3 units and the environment length is 216 steps. The final sparse reward is the Euclidean distance between the agent and the goal if the goal is not reached, otherwise a fixed reward of 1 penalized by a fraction of the number of steps taken, down to a minimum of 0.8.

**FourRooms.** A 14x14 unit space with a 6x6 room in each corner. Adjacent rooms are connected by a width-2 corridor along the outer edge of the space, i.e., there is a cross-shaped obstacle in the center. The agent starts in a random location and the goal is in the diametrically opposite location. The step size is 0.2 units and the environment length is 250 steps. The final sparse reward is the Euclidean distance between the agent and the goal if the goal is not reached, otherwise a fixed reward of 1 penalized by a fraction of the number of steps taken, down to a minimum of 0.8.

**SelectObj.** A 12x12 unit open space. The agent starts in the center. The near goal is 4 to 4.5 units away and the far goal is 5 to 5.5 units away. The two goals are 3 to 4 units away from each other. The step size is 0.05 units and the environment length is 200 steps. Unlike MazeS3 and FourRooms, SelectObj does not terminate upon reaching a goal. The final sparse reward is the Euclidean distance between the final agent position and the closest goal to the final position, plus a fixed reward of 1 for being within 1 unit of the original far goal.

### H.2 Compiler Phase Ordering

The action space consists of 46 different program transformations, and a trajectory consists of 45 transformations (quite short, considering many transformations have no effect unless applied in a specific order). The reward is the difference between the original and final number of execution cycles. Since the environment is deterministic, we only run 1 trial for each method. Thus far we have followed the setup in [15]; however, unlike [15], we allow a budget of only 50 trajectory queries.